Leave no trace: A non-destructive correlative approach providing new insights into impactites and meteorites

Martell, Josefin

2022

Document Version:
Publisher's PDF, also known as Version of record

LITHOLUND THESES 37

Leave no trace: A non-destructive correlative approach providing new insights into impactites and meteorites

JOSEFIN MARTELL
LITHOSPHERE AND BIOSPHERE SCIENCE | DEPARTMENT OF GEOLOGY | LUND UNIVERSITY 2022

LITHOLUND THESES 37

Leave no trace: A non-destructive correlative approach providing new insights into impactites and meteorites

Josefin Martell

LUND
UNIVERSITY

Lithosphere and Biosphere Science
Department of Geology

DOCTORAL DISSERTATION
by due permission of the Faculty of Science, Lund University, Sweden.
To be defended at Geocentrum II, Sölvegatan 12, Lund, room Pangea, on the 2nd of December, at 13:00.

Faculty opponent
Prof. Dr. Gordon Osinski
Western University, Canada

Cover image and illustrations: Josefin Martell

Lithosphere and Biosphere Science
Department of Geology
Faculty of Science

ISBN 978-91-87847-68-4 (print)

ISBN 978-91-87847-69-1 (pdf)

ISSN 1651-6648

Printed in Sweden by Media-Tryck, Lund University, Lund 2022

Organization

LUND UNIVERSITY
Department of Geology
Sölvegatan 12
SE-223 62 Lund
Sweden

Author: Josefin Martell

Document name

DOCTORAL DISSERTATION

Date of issue: 2nd of December, 2022

Sponsoring organization

Title and subtitle "Leave no trace: A non-destructive correlative approach providing new insights into impactites and meteorites"

Abstract

Impact cratering is today recognized as a fundamental geological process on all rocky bodies in the solar system. On Earth, however, processes such as plate tectonics and erosion have eradicated most craters from the geological record, or they may be buried under sediments, oceans, and vegetation. The formation of a hypervelocity impact crater involves extreme pressures and temperatures that induce permanent changes into the target rocks, so called shock-metamorphic effects, which can be used to identify and confirm impact structures.

The research in this thesis focuses on the impact cratering process, both during the formation, and post-impact. A number of terrestrial impactites and meteorites were analyzed using a multi-modal approach, including correlative non-destructive neutron and X-ray imaging, and detailed 2D analysis using scanning electron microscopy and electron backscatter diffraction. The material encompasses: (1) impactites from the Mien impact structure, (2) a sample of the Martian Miller Range (MIL) 03346 meteorite, (3) a Chicxulub drill core sample, (4) a sample of Libyan Desert Glass, and (5) a sample of impact melt rock from the Luizi impact structure.

The first study investigated shock deformation in zircon grains from the Mien impact structure in Sweden, using electron backscatter diffraction (EBSD). The results show that several of these grains contain evidence of the former presence of a high-pressure phase that is only known from impact structures. These grains would be suitable candidates for refining the age of the impact event. In paper II, combined NCT and XCT were employed to investigate the three-dimensional distribution of hydrogen-rich material in MIL 03346, by utilizing the neutrons' sensitivity to hydrogen. The results revealed that the hydrogen-rich material occurs in localized clusters, with limited interconnectivity between clusters. This suggests that the fluid source could be small patches of sub-surface ice and that the alteration event likely was short-lived, meaning that the source terrain of this sample was likely not habitable. In Paper III we combined XCT and NCT to test if these methods can be used to locate projectile material in impactites. After careful investigations of the 3D images, an iron-nickel silicide spherule could be pin-pointed in the Libyan Desert glass. The sample was then polished for detailed analysis using scanning electron microscopy. Overall, the non-destructive nature of XCT and NCT makes these methods highly relevant for studying rare samples, such as meteorites and returned samples.

Key words: Impact cratering; neutron tomography, X-ray tomography; impact structure, Mars, shock metamorphism

Classification system and/or index terms (if any)

Supplementary bibliographical information | Language

ISSN and key title: 1651-6648 LITHOLUND THESES | ISBN 978-91-87847-69-1

Recipient's notes | Number of pages 111 | Price

Security classification

Signature: Josefin Martell Date: 20/10-2022

Contents

List of papers

This thesis is based on the three papers listed below, which have been appended to the thesis. Paper I is reprinted under permission of John Wiley and Sons. Paper II is reprinted under the permission of AAAS.

Paper I
Martell, J., Alwmark, C., Holm-Alwmark, S., & Lindgren, P. (2021). Shock deformation in zircon grains from the Mien impact structure, Sweden *Meteoritics & Planetary Science, 56*(2), 362–378. [https://doi.org/10.1111/maps.13625].

Paper II
Martell, J., Alwmark, C., Daly, L., Hall, S., Alwmark, S., Woracek, R., Hektor, J., Helfen, L., Tengattini, A., & Lee, M. (2022). The scale of a martian hydrothermal system explored using combined neutron and x-ray tomography. *Science Advances, 8*(19), eabn3044. [https://doi.org/10.1126/sciadv.abn3044]

Paper III
Martell, J., Alwmark, C., Alwmark, S., Woracek, R., Hall, S., Ferrière, L., Daly, L., Bender-Koch C., Hektor, J., Helfen, L., & Tengattini, A. (2022). Combined neutron and x-ray tomography for detecting projectile material and hydrous constituents in planetary samples. *Manuscript*.

Acknowledgements

First of all, thank you, Carl, I cannot overstate how glad I am that I had you guiding me through this thesis work and for introducing me to the field of impact cratering. Maybe most importantly for everyday life, thank you for making it fun going to work, and for always being encouraging.

Sanna, thank you for being both a mentor and a good friend during the past few years. I have really been lucky to have such an inspiring scientist at my workplace, who also happens to be incredibly generous and supportive.

I'm also grateful to my co-supervisors, Luke Daly and Robin Woracek. As experts in your respective fields, you have brought creative ideas and practical help to the thesis projects. Thank you also for all feedback on manuscripts and proposals.

Thank you to all the amazing people in the planetary group for interesting science discussions and for contributing to a great atmosphere: Appe, Gabriel, Carl, Sanna, Paula, Maria, Leif, Anders and Uffe.

I owe great thanks to many of those whom I have been working with on the tomography projects. First, Stephen Hall for scanning countless samples and for teaming up on the meteorite project, and Sara Johansson for scanning even more samples and helping out with sample analysis. I'd likewise like to thank our beamline scientists (and co-authors on most papers and conference abstracts) at ILL, Alessandro and Lukas. Johan Hektor: you are a true inspiration when it comes to replying to emails (the fastest in academia?) for which I am very grateful… since I have sent you many emails. Thank you for helping me with everything tomography related.

I'm grateful to all co-authors, for inspiring discussions, feedback and comments on the manuscript, and for being patient with my last-minute emails, often named something like "URGENT" (or sometimes the slightly less stressful variant "semi-urgent!").

There are many people at the department, both current and former colleagues, that have made PhD life a lot easier, particularly Gert, everyone at the library, Johan Lindgren and Helena F for keeping track of my PhD studies, and of course, everyone at the kansli.

I would also like to thank Anders S for all opportunities to teach/mentor students in your courses, and for being an inspiring and enthusiastic lecturer and senior colleague.

Thank you, all PhD-students, both old (pre-pandemic) and new (post-pandemic), it has been great getting to know every single one of you. I have been lucky to have had great office mates: Ingrid, Cindy, Maria, Miguel (short but memorable), and Karolina. I also made many good friends: **Inda**, Gabriel, Appe, Miriam, Chiara, Miguel.

Thank you Inda, Chiara, Andrea, Robin, Victor for bringing me well-needed snacks during the past few days.

Finally, to the most important people in my life: mamma, pappa, Helena, Per (+Folke & John), Victor, thank you for always being curious, supportive, and emphatic.

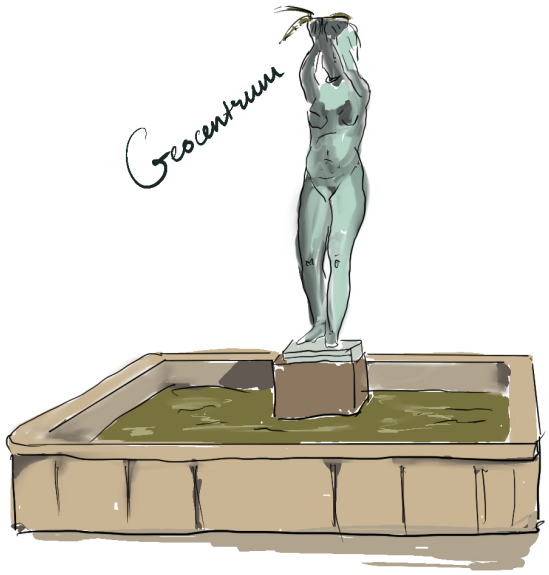

Basic definitions and abbreviations

Here are definitions and abbreviations of the most important terms used in this thesis.

Impact craters: General term that encompasses craters formed by all impacts of an extraterrestrial object, with or without evidence of shock metamorphism.

Hypervelocity impact *crater*: Morphological structure formed by a collision of two planetary bodies at, or near, cosmic velocity. Requires evidence of shock metamorphism in the target rocks.

(Hypervelocity) impact *structure*: Non-pristine impact crater, where the original crater morphology is modified or no longer present, e.g., due to erosion.

Shock metamorphism: Permanent deformation in minerals and rocks subjected to hypervelocity impacts.

Impactites: rock that was created or modified during a hypervelocity impact.

NCT: Neutron computed tomography

XCT: X-ray computed tomography

EBSD: Electron Backscatter Diffraction

SEM: Scanning electron microscopy

EDS: Energy dispersive spectroscopy

K–Pg boundary: Cretaceous–Paleogene boundary

Introduction

Impact cratering is today accepted as a fundamental geological process on all rocky celestial bodies in the solar system. Some of our closest neighbors, the Moon and Mars, have gotten their distinct appearance from millions of collisions since their formation, and although not as obvious on Earth, we know that meteorite impacts have influenced both the geological and the biological history of our planet; at least one mass extinction can be linked to a massive impact event (Alvarez et al. 1980; Smit and Hertogen 1980; Schulte et al. 2010). However, meteorite impacts are not merely destructive forces; they might in fact have been essential for life to emerge in the first place, by delivering the necessary building blocks for life to our planet (Osinski et al. 2020).

Since the Moon is the only celestial body whose cratered surface can be seen with the naked eye from Earth, it has inspired humans throughout history to reflect on our place in the universe: could the Moon be inhabited by other living creatures (e.g., Wilkins 1638)? How did it form, and why does it look so different from Earth? A major scientific breakthrough came when Galileo pointed a telescope at the Moon and created a detailed map of its surface. He thereby showed that it is not a smooth sphere, but has terrain similar to Earth (e.g., Koeberl 1999). Some centuries later, inventor and astronomer James Nasmyth began to carefully sculpt plaster figures based on observations made through a self-made telescope, which he then photographed and printed in the book *The Moon: Considered as a Planet, a World, and a Satellite* in the year of 1874. The photographs provide a spectacular view of the terrain that, although fake, was more realistic than any photographic technique at the time could achieve (Fig. 1).

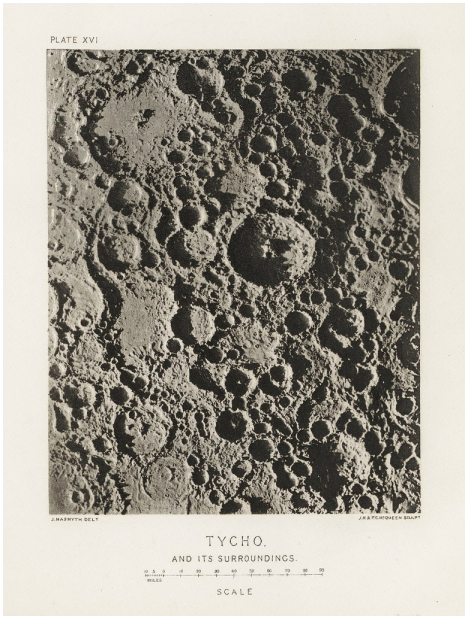

Figure 1. Plaster figure of the Tycho crater on the Moon. From the book *"The Moon: Considered as a Planet, a World, and a Satellite"* by James Nasmyth in 1874.

Impact cratering research in the 20th century

Although considered to be of minor importance, impact craters were recognized in the early 20th century. Mining engineer Daniel M. Barringer and his colleague Benjamin C. Tilghman suggested in 1905 that the spectacular Meteor Crater (sometimes called "Barringer Crater") in Arizona was produced by the impact of an iron-metallic meteorite (Barringer 1905) which was later confirmed by the findings of the quartz polymorph coesite (e.g., Chao et al. 1960). Nevertheless, it would take several decades until meteorite impacts were considered major contributors to Earth's geological history, and it was first when Apollo astronauts brought lunar rocks to Earth in the 1960 and 1970s, that it became widely accepted that the craters of the moon formed as the result of meteorite impacts rather than volcanic activity (Melosh 1989). The realization that the conditions during hypervelocity impacts can produce permanent and unique modifications to rocks and minerals, paved the way for the discovery and confirmation of impact structures on Earth (e.g., McIntyre 1962; Carter 1965; Stöffler 1966 and many others). Lunar rocks and other returned samples (e.g., from the Hayabusa mission; Yada et al. 2022) have advanced our knowledge of the Solar System; e.g., the Apollo samples have shed light on the origin of the moon (e.g., Wiechert et al. 2001; Zhang et al. 2012), and enabled surfaces of cratered bodies to be dated using "crater chronology", a crucial tool in understanding the evolution of other planets (e.g., Le Feuvre and Wieczorek 2011). The upcoming Mars Sample Return will likely be the next big leap in planetary science, aiming to answer fundamental questions about the origin of life and the early history of our solar system (e.g., Farley et al. 2020).

The future of impact cratering research is bright, and new technological advances have, and will continue to, expand the toolbox for investigating some of the most violent geological processes in the solar system by searching for the tiniest traces of impact.

Scope of the thesis

The motivation of this thesis was to explore how correlative imaging techniques can advance our understanding of the impact cratering process, both during crater formation and post-impact. The focus was on impactites, and to localize and characterize shock metamorphic features, hydrous minerals, and projectile material within these rocks. This was achieved by utilizing non-destructive neutron- and X-ray tomography, and electron backscatter diffraction.

More specifically, the work included in this thesis can be divided into four specific aims:

I. To employ a multimodal approach to pinpointing projectile material in impactites.

II. To explore the complementarity of neutron and X-ray tomography for investigating the distribution of hydrous phases in meteorites.

III. To gain insight into the impact cratering process through the identification of shock metamorphic features.

IV. To pave the way for using non-destructive techniques in light of upcoming sample return missions.

This thesis is based on three first-author papers, of which two are published, and one is manuscript form.

The chapters of this summary are intended to provide a broad context to the papers in this thesis.

Background

The impact cratering process

About 66 million years ago, a celestial body traveling at hypervelocity speed (>11 km/s) penetrated the Earth's atmosphere and unleashed the cataclysmic event that triggered the extinction of ~75% of all living species, including the non-avian dinosaurs (e.g., Alvarez et al. 1980; Smit and Hertogen 1980; Schulte et al. 2010). The projectile (most likely an asteroid; e.g., Quitté et al. 2007; Goderis et al. 2013) was large enough to remain coherent until it hit the surface of the Earth and caused permanent deformation in rocks and minerals, which is still detectable today (e.g., Bohor 1990; Kamo et al. 2011). These particularly energetic impact events form *hypervelocity impact craters* (Melosh 1989; Osinski et al. 2022). On Earth, the constant reworking of the crust, volcanism, burial, and erosion leads to an incomplete terrestrial impact record, biased toward young structures. To date, approximately 200 hypervelocity impact structures have been identified on Earth (Impact crater database 2022, impact.uwo.ca), and the oldest of these, the Yarrabubba impact structure in Australia, is "only" 2.2 billion years old (Erickson et al. 2020).

The formation of a hypervelocity impact crater begins the instant the projectile reaches the ground surface, and is usually divided into three stages: **(1)** contact and compression, **(2)** excavation, and **(3)** modification (Fig. 2A–E).

The contact and compression stage

The contact and compression stage is the briefest of the three stages: the initial contact between the projectile and the planet's surface (target), and the subsequent compression, takes place in a matter of milliseconds, meaning that in the blink of an eye, a single point on Earth can experience pressures of up to a thousand gigapascals (GPa; for comparison, the pressure at the centre of the Earth is ~360 GPa), extremely high strain rates, and temperatures of many thousands of degrees (e.g., Melosh 1989). The kinetic energy carried by an impacting object (projectile) only a few meters across is equivalent to that of an atomic bomb (French 1998). When the projectile reaches the ground surface, it will generate strong shock waves that propagate through, and compress, both the target and the projectile (Melosh 1989). As the shock waves propagate through the target rocks, they form a hemispherical pattern, and the pressure decreases steadily as the shock waves move away from the point of impact. Shock waves in the projectile will become rarefaction (release) waves as they reach the back end of the projectile, and when they reach the projectile-target interface, the entire projectile will vaporize and melt (Fig. 2A; Melosh 1989).

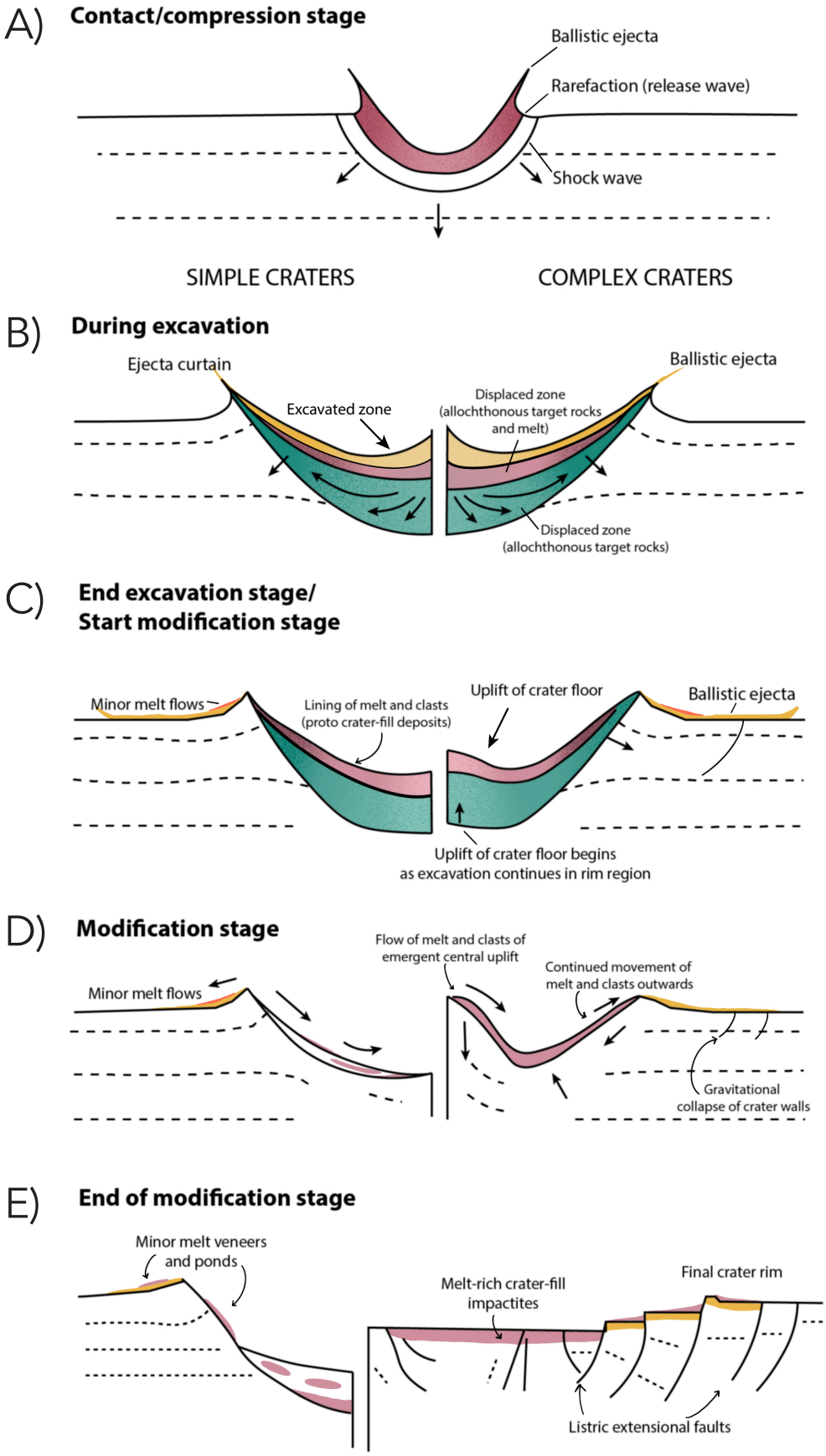

Figure 2. Formation of a hypervelocity impact crater in a non-marine target. The left part of the figure depicts the formation of a simple crater, and to the right the formation of a complex crater. A) The initial contact and compression stage. B-C) The excavation stage. A transient cavity forms as the target material is excavated and displaced. The transition to the modification stage of complex crater begins when the uplift starts to form. D-E) During modification, debris will fall inwards back into the crater in small (simple) craters. In complex craters, a collapse of the transient cavity will occur, and the crater floor will be uplifted (to a central uplift). E) Final crater form. Figure modified from Osinski and Pierazzo (2012) and Osinski et al. (2022).

The excavation stage

At this stage, the projectile has been vaporized and is no longer involved in the crater formation (Fig 2B–C). Vaporized target and projectile material may expand rapidly to form a vapor cloud/plume above the crater, parts of which in some cases can even exceed the escape velocity (Melosh 1989). The subsequent crater excavation takes place as the shock waves move through the rock, setting material into motion, and forming an "excavation flow field" that spreads out from the point of impact. Material thrown out of the crater only sample about 1/3 of the crater depth, abd material further down is pushed downward into the target, causing deformation of the underlying rocks. This process results in the formation of a "transient cavity"; material in the upper part of this zone ("excavated zone") is ejected ballistically beyond the crater rim, where it forms a continuous ejecta blanket. Material from below the excavated zone carries to little kinetic energy to be ejected, but will be displaced ("displaced zone") within the transient cavity (Fig. 2B; e.g., Melosh 1989).

The modification stage

When the shock and rarefaction waves no longer excavate or displace material, i.e., when the transient cavity has reached its "final" diameter, debris will move downward and back toward the crater center. The extent of the collapse can range from debris falling back into small, *simple* craters and forming a breccia lens, to formation of central peaks and terraced walls in larger, *complex* craters (Fig. 2D–E) (Melosh 1989). The degree of modification of the transient crater is controlled by e.g., the energy carried by the projectile (i.e., velocity and size of the impactor), gravity and material properties. The resulting crater can either be described as a *simple crater*, which are small, ~2–4 km (on Earth), bowl-shaped depressions with raised rims (Fig. 3), or as larger, >4 km (on Earth) *complex craters*, which form a central uplift (Fig. 3; French 1998). Large, complex craters can display peak-rings that are thought to form from a process involving inward-collapsing rim material that collides with an over-steepened central peak (Fig. 3; Baker et al. 2016; Gulick et al. 2020). Multi-ring basins are an elusive crater morphology; they are the largest impact craters in the solar system, and have characteristic rings surrounding a central, flat basin (Fig. 3; Potter 2015).

While the three phases describe the formation of hypervelocity impact craters, long-term crater modification, caused by e.g., lithostatic crustal relaxations and erosion can continue over millions of years (e.g., Kenkmann et al. 2012). In Paper II we discuss one of these major post-impact processes, namely impact-induced hydrothermal systems.

Impact-induced hydrothermal systems

A hydrothermal system is, in its most general sense, hot water circulating through the bedrock, and it thus requires a heat source, permeable host rock, and a fluid source. On Earth, hydrothermal systems are mainly associated with volcanic areas, but impact-generated heat from an impact melt sheet can similarly drive the circulation of hot fluids if the target rock contains water or ice (Farmer 2000; Abramov and Kring 2005; Osinski et al. 2013). Although pressures and temperatures reached near the point of impact during crater formation are high enough to eradicate life in the immediate surrounding, these extreme conditions rapidly decay with distance from the center (e.g., Ramkissoon et al. 2021). The cooling history of the heated impactites depends on the size of the crater and the nature of the target rock (Abramov and Kring 2005; Cockell 2006), but the lifetime of an impact-induced hydrothermal system can be thousands of years, and in large-scale impacts, up to millions of years (e.g., 1 Ma for the Sudbury impact structure; Ames et al. 1998; Schmieder and Jourdan 2013). Impact-induced hydrothermal systems were likely important sub-surface refugia for organisms early in the Earth's history, during a time when cataclysmic meteorite impacts might have vaporized the Earth's oceans for long periods (Kring 2003). On Earth, heterotrophic microorganisms have been found in shocked gneiss from the Haughton impact structure in the Arctic (Cockell 2004). Shocked rocks offer UV shielding and retain moisture (Cockell et al. 2003; Kring 2003) and are favorable for deep and long-lasting microbial colonization, at depths of several kilometers (Kring 2000; Kring and Cohen 2002). There is increasing evidence that Mars hosted habitable conditions throughout the Noachian (about 4.1 to 3.7 billion years ago), and impact-generated hydrothermal systems could have continued to support life forms as the Martian surface began to lose its water (Ramkissoon et al. 2021). Shocked rocks could,

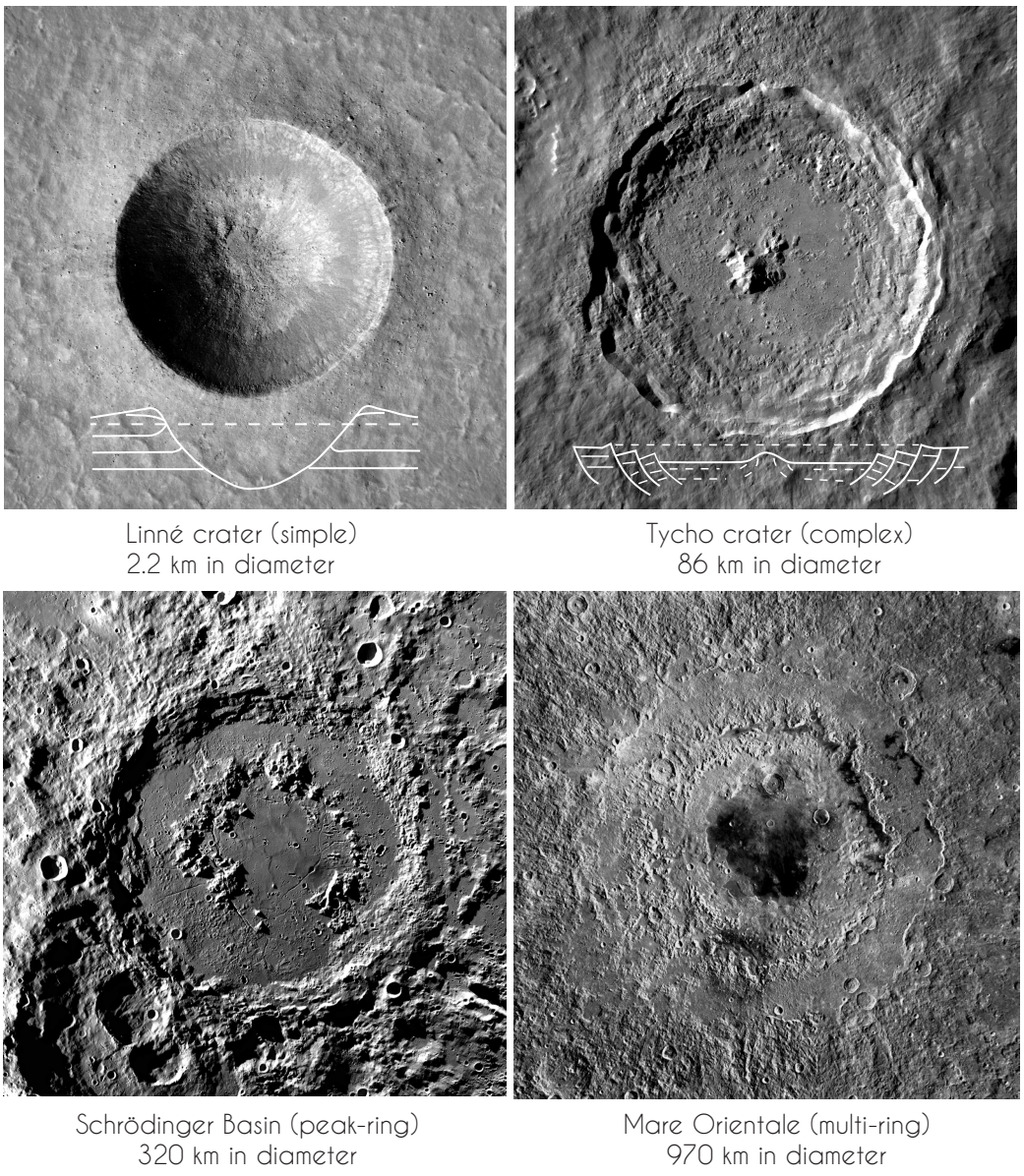

Figure 3. A comparison between four crater morphologies. A schematic illustration on the images of Linné and Tycho crater depicts a cross-section of these crater types. The dotted line represent the original ground surface. All photos are from the Lunar Reconnaissance Orbiter Camera (NASA/GSFC/Arizona State University). The illustrations are modified from Osinski et al. (2012).

thus, be prime targets for exploring traces of life on other planets than Earth.

Hydrothermal alteration refers to the chemical weathering of minerals, caused by their interaction with warm water that has a temperature above the local geothermal gradient (e.g., Osinski et al. 2013). Outside Earth, aqueously altered minerals have been found e.g., in Martian meteorites (e.g., Gooding et al. 1991; Treiman et al. 1993), and on the Martian surface (e.g., Mustard et al. 2008; Farley et al. 2022). Osinski et al. (2013) suggested a division of impact-generated hydrothermal minerals into either 1) primary hydrothermal minerals precipitated from solutions, 2) secondary assemblages formed by the alteration of primary hydrothermal minerals, or 3) hydrothermally-altered target-rock assemblages. The nature of the mineral assemblages is influenced by the target lithology and the hydrothermal fluids and can provide insight into the nature of the hydrous activity, as well as the longevity of the system (Osinski et al. 2013). Based on the simple mineralogy of secondary assemblages of the "SNC" (Shergotty-Nakhla-Chassigny) Martian meteorites, Bridges et al. (2001) suggested a short-lived hydrothermal system with low-temperatures (25–150°C). More long-lived systems are generally expected to result in a higher degree of alteration and more extensive hydrothermal deposits (Osinski et al. 2013).

Impactites

Impactite (also "impact rock") is a general term for all rocks shaped or formed by shock waves or other processes taking place during a hypervelocity impact (Grieve and Therriault 2012). The result can be everything from breccias with melt particles, thick melt sheets, and glassy fragments (both distal and proximal), and they in many cases contain evidence of shock metamorphism. During the excavation stage of an impact, most target rocks are subjected to shock pressures of >25 GPa (French 1998), resulting in a mixture of vapor, highly shocked (but coherent) rocks, and rock melts (Grieve and Therriault 2012). Depending on the distance to the point of impact, the target material is either ejected from the transient crater or remains within the structure. The classification of impactites changes with new interpretations and knowledge, but generally, it is based on the lithological character of the rock, such as particle size, source material, the relative percentage of different components (melt, matrix, and inclusions), and the source location (Grieve and Therriault 2012). They are further grouped by whether they have remained in their original, pre-impact, location or if they have been transported by the crater flow field or during the modification stage (e.g., Grieve and Therriault 2012). Impactites that have remained in their original location are called *autochthonous*; these are fractured rocks found in the rim areas of both simple and complex craters. *Parautochthonous* impactites are found on the crater floor in simple structures, and have been moved from their original location, but appears to be in place. They often contain shock metamorphic features that record pressures of up to ~25 GPa around the centre of the structure. In complex craters, the parautochthonous target rock is uplifted to surface positions during the modification stage. *Allochthonous* impactites have been displaced from their original location (formed elsewhere and clearly moved to their current location), and can be either proximal or distal, depending on if they remain within or around the final crater or if they are ejected out of the crater. Proximal, allochthonous impactites include impact breccias and impact melt rocks (Grieve and Therriault 2012). Impact breccias without melt particles make up the main part of the crater fill in simple structures. In complex structures, especially in crystalline targets, a higher percentage of the target rock will be melted and thus mixed with the impact breccias, which is generally found below the impact melt sheet. Melt-bearing breccias are generally polymict with clasts of impact glass and lithic clasts in a clastic matrix. In complex impact structures that are formed in crystalline targets, the *parautochthonous* target rock is covered by a coherent sheet of impact melt rock. Impact melt rock can also occur as dikes in complex structures of crystalline targets (Grieve and Therriault 2012). As the name suggests, the impact melt rocks have a melt matrix, which is either crystalline, glassy or devitrified glass, depending on the cooling history, and with a composition close to that of the target rocks (Grieve and Therriault 2012). The melt matrix is mixed with varying degrees of mineral and lithic clasts, and based on the clast content they can be referred to as either clast-rich or clast-poor impact melt rocks (Stöffler et al. 2018). Historically, impact melt rocks have often been mistaken for being of volcanic origin, e.g., the "Mien rhyolite" in the Mien impact structure in Sweden (Holst 1890; see discussion in Martell et al. 2021b). Distal allochthonous impactites always refer to ejecta, and include air-fall deposits, tektites and impact glass (Grieve and Therriault 2012; Stöffler et al. 2018). In some cases, this ejecta can be traced back to the source crater, for example, distal ejecta (e.g., accretionary lapilli, spherules, and shocked quartz) from the Sudbury impact structure has been found approximately 400–900 km from the source crater (e.g., Cannon et al. 2010). Sometimes, it is not possible to identify a source crater; perhaps because the source crater has been removed by erosion or covered by post-impact geologic activity. In these cases, ejecta deposits might be the only remaining "evidence" of an impact event, and can give valuable information about impact events early in the Earth's history (Koeberl et al. 2015).

Physical fragments of the projectile rarely survive the (hypervelocity) impact process, but a meteoritic component can be preserved in the target rock in the form of a small amount of melted and recondensed projectile material (generally less than 1 wt%; Goderis et al. 2012a). Impact melt rocks are typically the most enriched in projectile material (Palme et al. 1978), but also other impactites can contain an extraterrestrial signal, as documented for the K–Pg boundary layer (Alvarez et al. 1980; Smit and Hertogen 1980). Identification of projectile material is usually done by detecting enrichments of certain siderophile elements, such as the platinum group elements (PGEs; Ru, Rh, Pd, Os, Ir, Pt) alongside more moderate siderophile elements such as nickel, chromium and cobalt, and by atypical isotopic ratios. Besides the K–Pg boundary layer, me-

teoritic components have been identified in e.g., the Chesapeake Bay impact structure (Lee et al. 2006), the Clearwater Lake impact structures (Grieve 1978), and in Lunar samples from the Apollo 15 and 16 landing sites (Liu et al. 2015), based on Re-Os isotope systematics and trace elements. Precise identification of the projectile, down to the meteorite class, has only been constrained for about 10 impact structures on Earth (Goderis 2011). One major issue in studies aimed at constraining the impactor type is that the inhomogeneous distribution of the material, most likely in the form of PGE nuggets, requires large sample volumes for their detection, and the exact processes governing the incorporation of meteorite material are still not known (Koeberl 1998; Goderis et al. 2012a). Consequently, the inhomogeneous distribution can result in a nugget effect (e.g., Tagle et al. 2004; Lee et al. 2006) that can lead to under- and overestimation of the PGE concentration for the whole rock, and furthermore to that projectile material is easily missed depending on sample size. In this thesis (Paper III), we investigate whether it is possible to locate project material in impactites using non-destructive methods. If possible, it would both provide knowledge about what happens during the incorporation of meteoritic material in impactites, and circumvent issues with whole-rock methods for determining projectile type for impact structures.

Shock metamorphism

Shock metamorphic features are permanent, residual effects that develop in rocks and minerals during hypervelocity impacts, and thus occur in both terrestrial and extraterrestrial rocks that were subjected to impact cratering. The deformation is caused by the shock wave as it transits the mineral, leading to a sudden increase in pressure that exceeds its Hugoniot elastic limit (HEL), which for most minerals is in the range between 1–10 GPa. The enormous pressure increase, and subsequent pressure release, lasts for less than a second, and the process is unique in nature to hypervelocity impacts. A comparison between static, endogenous metamorphism of the terrestrial crust (which rarely reaches pressures of about 1–2 GPa) and shock metamorphism can be illustrated by a pressure-temperature (P-T) plot (Fig 4). Shock experiments have demonstrated how the response of several minerals (e.g., quartz, zircon) changes with shock pressure and how these minerals can be used as shock barometers. Several factors can influence peak pressure and temperature in impacted materials, such as high porosity or fractures in-between grains, which can cause local pressure excursions up to a magnitude higher than the shock front peak pressure (Sharp and DeCarli 2006).

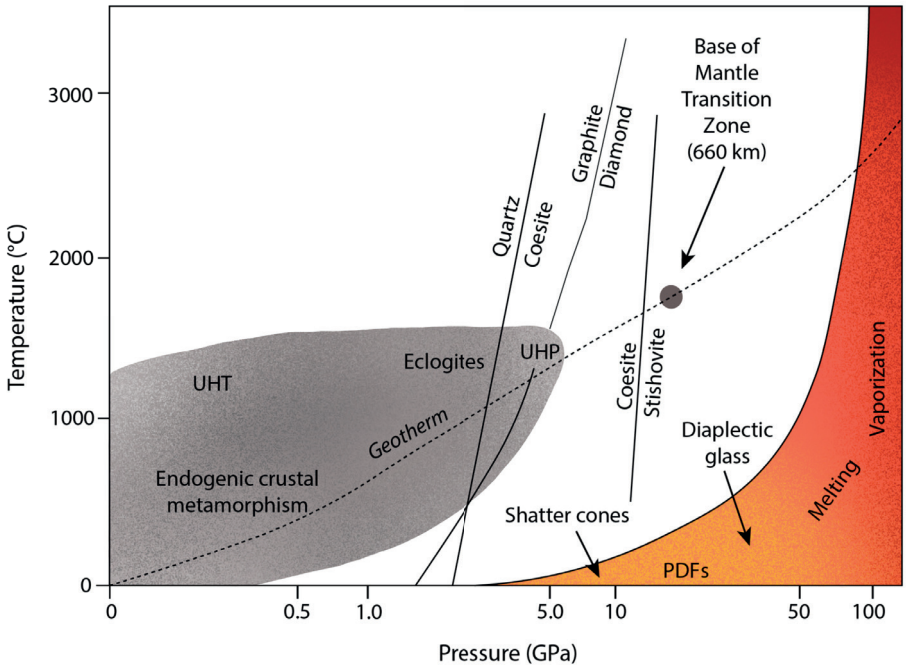

Figure 4. A pressure-temperature plot showing conditions during "normal" endogenic crustal metamorphism (gray), and conditions during shock metamorphism (orange-red). In the figure are also show where some different shock metamorphic features form (e.g., planar deformation features), as well as the transition between three high-pressure polymorphs. The pressure axis is logaritmic. Modified from French (1998) and Osinski et al. (2022).

Shock-metamorphic features can be seen at both the macro- and microscales, with shatter cones (macroscale), phase transformations (e.g., zircon to reidite and quartz to stishovite), and mechanical deformation in minerals being the most common (Stöffler et al. 2018). Planar deformation features (PDFs) in quartz have been reported from nearly all terrestrial impact structures and remain the most commonly used shock diagnostic feature (e.g., Engelhardt and Bertsch 1969; Stöffler and Langenhorst 1994; Grieve et al. 1996; French 1998; French and Koeberl 2010). PDFs are thin, straight lamellae that develop in specific crystallographic planes. The orientation of these planes corresponds to different shock pressures (e.g., Grieve 1997), which have been used to constrain the shock barometry of e.g., the Slate Island impact structure (Dressler et al. 1998), and the Siljan impact structure in Sweden (Holm et al. 2011).

The mineral zircon ($ZrSiO_4$) is a common accessory mineral in many terrestrial rocks, and due to its capability as a U-Pb geochronometer, zircon has been used to constrain the age of several impact structures, such as the Sääkasjärvi structure in Finland (Kenny et al. 2020), and the Yarrabubba impact structure in Australia (Erickson et al. 2020). Compared to many other minerals, zircon is resistant to alteration and can thus remain in the geological record for a long time; zircon from Jack Hills in Australia has yielded U-Pb ages of ~4.4 Ga, making these grains the oldest minerals so far found on Earth (Wilde et al. 2001). Zircon can display a variety of shock microstructures such as mechanical twins (along {112}; Moser et al. 2011; Timms et al. 2012; Erickson et al. 2013), {100}-parallel deformation bands (Timms et al. 2012; Erickson et al. 2013), granular textures (e.g., Bohor et al. 1993; Schmieder et al. 2015; Martell et al. 2021b) decomposition of zircon to ZrO_2 and SiO_2 (El Goresy 1965), and conversion to the high-pressure phase reidite (Glass and Liu 2001). Reidite has been found in a number of impact structures (e.g., Glass et al. 2002; Wittmann et al. 2006; Cavosie et al. 2015; Reddy et al. 2015; Plan et al. 2021), and can be identified using e.g., Raman spectroscopy (e.g., Knittle and Williams 1993; Gucsik 2007) and electron backscatter diffraction (EBSD) techniques (Cavosie et al. 2015; Plan et al. 2021). In recent years, technical advances using EBSD have resulted in the identification of systematically oriented zircon neoblasts, that are expressed as 90° clusters when plotted in a pole figure, so-called FRIGN (Former Reidite in Granular Neoblasts) zircon (Erickson et al. 2017; Cavosie et al. 2018a). The neoblasts form as the reidite reverts back to zircon, and FRIGN zircon is thus considered a "phase heritage" (Cavosie et al. 2020) and can be used as a shock-indicator. In Paper I, we report the findings of shock metamorphosed zircon in impacites from the Mien impact structure (see Martell et al. 2021b). Shock experiments have shown that the phase transition to reidite occurs at pressures of ~30 GPa and is completed by 52 GPa (Kusaba et al. 1985; Fiske 1999; Leroux et al. 1999). The identification of shock metamorphic features is thus not just a method to confirm impact structures; the unique response of minerals to hypervelocity impacts offers a window into a process we have never experienced first-hand.

Methods

Imaging methods in planetary science

Optical microscopy and scanning electron microscopy (SEM) are two invaluable tools for e.g., petrographic descriptions and the identification of shock metamorphic features in minerals. For example, PDFs in quartz are easily observed by means of optical microscopy (e.g., Stöffler and Langenhorst 1994; French 1998), and SEM can be employed to retrieve detailed compositional information about a mineral (e.g., Treiman 2005). However, sample preparation often involves crushing the sample for manual picking of minerals or whole-rock analysis, dissolving the sample in acid to separate e.g., heavy minerals, or cutting the sample to produce thin sections. Concequently, the mineralogical context is either lost or limited to a 2D view, which might not be fully representative of the rock. Furthermore, for especially valuable material, such as meteorites and returned samples, sample loss must be kept to an absolute minimum. In this thesis, alternative and/or complementary, imaging techniques have been explored. This chapter includes a short review of the three main techniques utilized within the scope of this thesis, followed by a method description of how the data was collected and processed.

Electron backscatter diffraction (EBSD)

Electron backscatter diffraction (EBSD) is a scanning electron microscopy (SEM) based technique that can be used to obtain quantitative mineral information on, e.g., grain size, grain orientation, strain gradient measurements, textures, and phase identification. Since the EBSD detector collects phase data based on the crystal structure of a mineral rather than the composition (compared to e.g., energy dispersive spectroscopy analysis; EDS), it is, for example, possible to distinguish between different polymorphs.

EBSD is nowadays routinely used in the Earth sciences (e.g., Prior et al. 2009). Applications to planetary materials include, e.g., investigations into petrofabrics in Martian meteorites (Daly et al. 2019b; Griffin et al. 2022), the identification of high-pressure polymorphs (Cavosie et al. 2018a), and shock deformation (Erickson et al. 2013). Shock experiments help us to understand under which conditions these features/polymorphs form, and thus, the EBSD analysis can give insights into the geological history of an impact structure.

To collect EBSD patterns, an electron beam is focused on a tilted (70°) sample surface, and the incident electrons will interact with the atoms in the sample and diffract among the crystallographic planes. Some diffracted electrons incident on specific atomic planes, at angles that fulfil the Bragg equation. The diffracted electrons can be detected on a fluorescent screen, where visible lines, so called "Kikuchi bands" or "EBSPs" (electron backscatter patterns) appear. These patterns are related to the geometry of the lattice planes in the crystal and thus give information about the crystal structure and orientation of the crystal. The patterns are indexed using a database with crystallographic information about different minerals. Further post-processing analysis is done with dedicated software. In Paper I and Paper II, we investigated shock deformation in zircon grains from the Mien impact structure, and augite crystals in a Martian meteorite, respectively.

Sample preparation

In Paper I, the investigated zircon grains were either handpicked and imaged as individual grains, or as part of thin sections. For picking of individual mineral grains, the impactite samples were crushed into a powder, from which zircon grains are separated by water-based gravitational separation using a Wilfley water shaking table (following the method by Söderlund and Johansson 2002). The zircon grains were then handpicked using a binocular microscope and cast in epoxy. The Martian meteorite sample was simply cast in epoxy without prior treatment. To collect high-quality EBSP patterns, the sample has to be polished flat. This is done by grinding the surface with increasingly finer grinding paper to remove scratches, and finally polishing the sample on a soft polishing cloth with colloidal silica in a NaOH dispersion. Our samples were also coated with a ~5 nm layer of carbon (a thicker layer will obstruct the beam) to avoid charging effects. After polishing, the sample was attached to a pre-tilted sample holder at an angle of 70° and inserted into the SEM chamber.

Acquisition

Both SEM and EBSD data were acquired at the Department of Geology, Lund University, Sweden using a Tescan Mira3 High-Resolution Schottky field-emission SEM, equipped with an Oxford Energy-Dispersive X-ray Spectroscopy (EDS) system a cathodoluminescence system, and an EBSD detector (Symmetry S2, Oxford Instruments), operating at 20 kV, with a working distance of 20 mm and a beam current of ~10 nA. More detailed acquisition details, such as step sizes for each measurement, are given in the method section of each paper.

Data processing

Post-processing was done using the software Channel 5, which allow constructing phase maps, visualization of misorientation between e.g., grains or neoblasts (i.e., the change in orientation from one feature to another), and intra-grain deformation.

Neutron and x-ray tomography

Combined neutron- and X-ray tomography was conducted on samples in papers II-III.

Neutron- and X-ray tomography (XCT/NCT) are non-destructive imaging techniques, used to study the interior of samples while requiring minor, or no, sample preparation. As such, they are ideal for inves-

tigating particularly sensitive and rare samples, e.g., from museum collections or extraterrestrial, returned samples (e.g., Blumenfeld et al. 2015; Mannes et al. 2015; Hanna and Ketcham 2017). Furthermore, by conducting an initial scan of a sample, later destructive analyses can target specific regions-of-interest-that might have been missed by random cutting of the sample for making thin sections. Scanning the sample also enables, e.g., quantification of internal porosity, distribution of different minerals, and fracture systems within a sample (Tengattini et al. 2020a).

X-rays were discovered already in 1895 by Wilhelm Röntgen (who was awarded a Nobel prize for the discovery) and were immediately put into practice for medical imaging purposes (Hessenbruch 2002). Neutrons were discovered by James Chadwick in 1932 (Chadwick 1932), almost four decades after X-rays. The discovery awarded him the Nobel Prize shortly after, but the development of neutron applications took a halt due to the Second World War. New progress was made in the mid-1950s when Thewlis utilized a neutron beam from the BEPO reactor at Harwell for neutron imaging (Brenizer 2013; Rogers 2013).

Previous studies in planetary science using NCT and XCT

X-ray imaging has been utilized for analyses of planetary materials since the 1980s, and has, during the last two decades, become a routine method to study the interior of planetary samples (Hanna and Ketcham 2017). Investigated materials range from meteorites and terrestrial impactites to returned samples, including 3D reconstructions of the interior of Apollo samples (Zeigler et al. 2014; Blumenfeld et al. 2015), petrography and petrofabrics of different types of chondrites (e.g., Krzesińska 2011; Friedrich and Rivers 2013; Hezel et al. 2013; Matsumoto et al. 2013) and impactites (Koeberl et al. 2002; Zubov et al. 2021), fracture networks in the Nakhla Martian meteorite (Needham et al. 2013) and a study of inclusions in chromite (Alwmark et al. 2011), but the number of XCT studies in planetary science exceed far beyond this list (an extensive review is given in Hanna and Ketcham 2017). In contrast, NCT has only been utilized in a limited number of studies of planetary materials, and most of these are relatively recent, in part due to the rarity of neutron facilities compared to XCT systems, which are available at several thousands of research institutions (Tengattini et al. 2020b). Previous NCT investigations include imaging of different types of chondrites (Hess et al. 2011; Pakhnevich 2016; Treiman et al. 2018; Needham et al. 2020), structural characterization of iron meteorites (Peetermans et al. 2013; Caporali et al. 2016) and investigations of impactites (Steen Duchnik et al. 2012; Fedrigo et al. 2018; Martell et al. 2021a), where the last is the precursor to paper III in this thesis.

Interaction with matter

X-rays interact with the electrons in the atom shell; on the contrary, neutrons lack electrical charge and interact with the nucleus of the atom. The interaction probability (cross-section) of neutrons is thus not dependent on the number of electrons of a specific atom, while for X-rays it follows a linear relationship with the atomic mass (Fig. 5; Kardjilov et al. 2006). The differences in cross-sections make neutrons and X-rays highly complementary; the neutron attenuation of light elements such as hydrogen is several orders of magnitude higher than the X-ray attenuation for the same element, while other heavier elements, for example, metals such as aluminum and lead, are practically transparent to neutrons (Tengattini et al. 2020b). A classic example illustrating this is an experiment showing a lead container containing a lily; the lead effectively blocks X-rays from penetrating the container, while the neutrons instead image the organic (hydrogen-rich) material within the container (Fig. 6).

The neutrons' ability to image the hydrogen within different materials has found many applications in, e.g., archaeological (Kardjilov et al. 2006; Mannes et al. 2015), paleontological (Pakhnevich et al. 2018), and medical sciences (Floyd et al. 2004), where distinguishing organic material is often important. Since neutrons interact with the nucleus of the atom, they are also sensitive to different isotopes. This has been utilized in 3D visualization experiments of water uptake in plants where heavy water (D_2O) has been used as a contrast agent to H_2O (Kardjilov et al. 2018).

The interaction between X-rays and neutrons with matter also depends on the energy of the applied radiation. For neutron imaging, thermal or cold (meV) neutrons are generally used, while X-ray energies in X-ray imaging are typically in the order of ten to several hundred keV (Kardjilov et al. 2006), making neutrons far less invasive in terms of radiation damage (Tengattini et al. 2020b). Neutrons are generated either by spallation in accelerator-driven

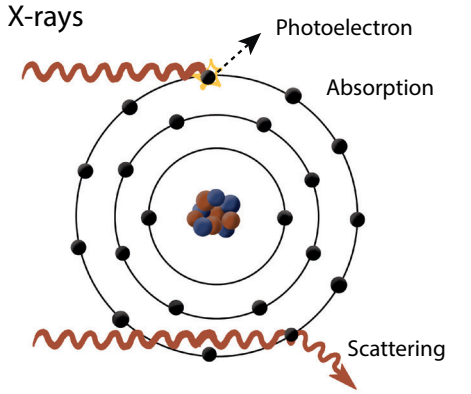

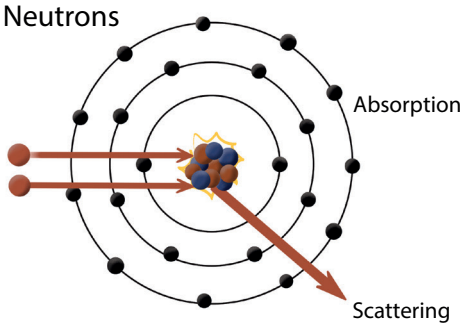

Attenuation coefficients for X-rays (cm^{-1}) (150kV)

1a	2a	3b	4b	5b	6b	7b	8	1b	2b	3a	4a	5a	6a	7a	0
H															He
0.02															0.02
Li	Be									B	C	N	O	F	Ne
0.06	0.22									0.28	0.27	0.11	0.16	0.14	0.17
Na	Mg									Al	Si	P	S	Cl	Ar
0.13	0.24									0.38	0.33	0.25	0.30	0.23	0.20
K	Ca	Sc	Ti	V	Cr	Mn	Fe	Co	Ni	Cu	Zn	Ga	Ge	As	Se	Br	Kr
0.14	0.26	0.48	0.73	1.04	1.29	1.32	1.57	1.78	1.96	1.97	1.64	1.42	1.33	1.50	1.23	0.90	0.73
Rb	Sr	Y	Zr	Nb	Mo	Tc	Ru	Rh	Pd	Ag	Cd	In	Sn	Sb	Te	I	Xe
0.47	0.86	1.61	2.47	3.43	4.29	5.06	5.71	6.08	6.13	5.67	4.84	4.31	3.98	4.28	4.06	3.45	2.53
Cs	Ba	La	Hf	Ta	W	Re	Os	Ir	Pt	Au	Hg	Tl	Pb	Bi	Po	At	Rn
1.42	2.73	5.04	19.70	25.47	30.49	34.47	37.92	39.01	38.61	35.94	25.88	23.23	22.81	20.28	20.22		9.77
Fr	Ra	Ac	Rf	Ha													
	11.80	24.47															

	Ce	Pr	Nd	Pm	Sm	Eu	Gd	Tb	Dy	Ho	Er	Tm	Yb	Lu
*Lanthanides	5.79	6.23	6.46	7.33	7.68	5.66	8.69	9.46	10.17	10.91	11.70	12.49	9.32	14.07
	Th	Pa	U	Np	Pu	Am	Cm	Bk	Vf	Es	Fm	Md	No	Lr
**Actinides	28.95	39.65	49.08											

Attenuation coefficients for thermal neutrons (cm^{-1})

1a	2a	3b	4b	5b	6b	7b	8	1b	2b	3a	4a	5a	6a	7a	0
H															He
3.44															0.02
Li	Be									B	C	N	O	F	Ne
3.30	0.79									101.60	0.56	0.43	0.17	0.20	0.10
Na	Mg									Al	Si	P	S	Cl	Ar
0.09	0.15									0.10	0.11	0.12	0.06	1.33	0.03
K	Ca	Sc	Ti	V	Cr	Mn	Fe	Co	Ni	Cu	Zn	Ga	Ge	As	Se	Br	Kr
0.06	0.08	2.00	0.60	0.72	0.54	1.21	1.19	3.92	2.05	1.07	0.35	0.49	0.47	0.67	0.73	0.24	0.61
Rb	Sr	Y	Zr	Nb	Mo	Tc	Ru	Rh	Pd	Ag	Cd	In	Sn	Sb	Te	I	Xe
0.08	0.14	0.27	0.29	0.40	0.52	1.76	0.58	10.88	0.78	4.04	115.11	7.58	0.21	0.30	0.25	0.23	0.43
Cs	Ba	La	Hf	Ta	W	Re	Os	Ir	Pt	Au	Hg	Tl	Pb	Bi	Po	At	Rn
0.29	0.07	0.52	4.99	1.49	1.47	6.85	2.24	30.46	1.46	6.23	16.21	0.47	0.38	0.27			
Fr	Ra	Ac	Rf	Ha													
	0.34																

	Ce	Pr	Nd	Pm	Sm	Eu	Gd	Tb	Dy	Ho	Er	Tm	Yb	Lu
*Lanthanides	0.14	0.41	1.87	5.72	171.47	94.58	1479.04	0.93	32.42	2.25	5.48	3.53	1.40	2.75
	Th	Pa	U	Np	Pu	Am	Cm	Bk	Cf	Es	Fm	Md	No	Lr
**Actinides	0.59	8.46	0.82	9.80	50.20	2.86								

Figure 5. X-rays and neutrons have different attenuation coefficients for different elements. Top: the X-rays interact with the electrons of the atoms, and the attenuation therefore increases with the atomic number. This is highlighted in the period table, where darker shades correspond to higher attenuation. On the contrary, neutrons interact with the nuclei, and the attenuation coefficient is thus not dependent on the number of electrons of an atom. Because of this, many neigbouring elements can be distinguished from one another. Iridium and hydrogen are highlighted in the periodic tables (red box). In contrast to X-rays, neutrons are sensitive to hydrogen, while both modalities have high iridium attenuations. Figure modified from Tengattini et al. 2020

facilities (Kardjilov et al. 2006) or by nuclear fission (Tengattini et al. 2020b). At a spallation source, neutrons are generated by accelerating protons towards a heavy-metal target, e.g., lead, causing neutrons to be emitted as the protons hit the target nuclei. In nuclear fission. In both cases, the neutrons need to be slowed down to be applicable for imaging purposes, which is usually done by leading them through "moderators". These generally consist of hydrogen or hydrogenous materials at low temperatures (Tengattini et al. 2020b). X-ray experiments can be conducted both in large-scale facilities (synchrotrons) and in lab-sized X-ray scanners. At synchrotrons, free electrons are accelerated to high velocities in a storage ring. X-ray radiation is generated from the electrons when their direction is modified, e.g., by undulators and wigglers (an insertion device) or by bending magnets, which forces the electrons to emit X-ray radiation. In lab-sized XCT systems, electrons are accelerated toward a metal target, and the interaction will generate X-ray photons.

Sample preparation

The acquisition requires no sample preparation; the sample is simply transferred to a sample holder. In our experiments, the size and type of sample holder (plastic for XCT and metal for NCT) differed depending on, e.g., the geometry of the sample and the number of samples scanned in each scanning session; in the latter case, samples were separated by a few layers of tinfoil. All samples were scanned with high-resolution X-ray imaging at the 4D imaging lab in Lund following the NCT. Potential epoxy embedding has to be removed before the NCT; this was the case for the Chicxulub drill core sample, which had a small amount of epoxy left on the surface when we first received it. Epoxy embedding is, however, not an issue for XCT, so if a sample would benefit from

epoxy embedding at a later stage of the investigation, NCT should be conducted before.

Acquisition

Neutron data was acquired at the ICON beamline at PSI in Switzerland (beamline specifics in Kaestner et al. 2011), and at the NeXT beamline at ILL in France (beamline specifics in Tengattini et al. 2020a). Both beamlines utilize cold neutrons at slightly different wavelength spectra. Following the neutron tomography, complementary X-ray imaging was conducted at the 4D imaging lab in Lund, Sweden. Voxel sizes for both modalities varied between 7 µm to 45 µm; the obtained voxel size for each sample was mainly due to a compromise between the allocated beam time, the sample size, and the signal-to-noise ratio.

In short, the sample is placed on a rotation stage, and radiographic projections are collected at different angles while the stage is rotated. At the same time, a detector measures the decrease in intensity between the incident beam and the final intensity after traversing the sample (i.e., the attenuation). The attenuation is dependent on the interaction between the X-ray photons/neutrons and the sample, and the amount of material traversed. The radiographs are then transformed into a set of 2D slices by reconstruction algorithms such as filtered backprojection. The resulting slices are "stacked" so that they can be visualized as a 3D volume, with grey scales corresponding to the attenuation of each voxel.

Data processing

Reconstruction of the images was performed at the neutron facility (Institut Laue Langevin and Paul Scherrer Institut respectively) using filtered backprojection. Back in Lund, the reconstructed images were aligned (or "registered") using the open-source software SPAM (Stamati et al. 2020). Fiji/ImageJ (Schindelin et al. 2012) was used to down sample the datasets for an initial, coarse registration, which decreases the computing time. The images were then loaded into SPAM for multi-modal image registration. A "by-product" of registration using SPAM is that it generates a phase segmentation based on a joint histogram, which provides a first indication of the character of the sample. After a coarse registration, the registration was refined using the full dataset.

After registering the NCT and XCT images, image segmentation (classifying voxels into different categories based on attenuation) and visualization were conducted using Dragonfly ORS (Dragonfly 2021.1 [Computer software] 2021). The registered images can be compared slice-by-slice, which allows segmentation based on the attenuation of different phases. Dragonfly generates a bivariate histogram, where the X-ray and neutron attenuation in each voxel is plotted as a point, and this histogram can be used for simple phase segmentations. Due to overlapping attenuations of some materials in the samples, we also manually segmented several minerals based on their crystal shapes, e.g., the greyscales of the rims in some olivine and augite grains in the Martian meteorite sample overlapped with parts of the mesostasis. The segmentation was compared with the results from SEM-EDS imaging- and compositional analysis of 2D sections of the samples.

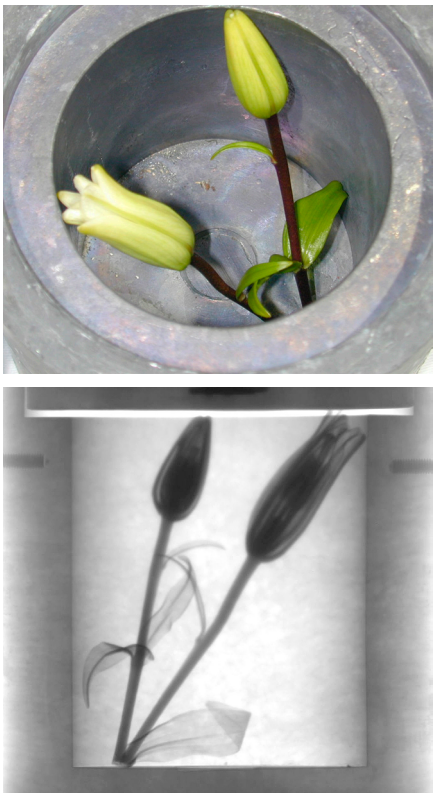

Figure 6. Neutron image of lilies inside a lead cask. The image demonstrates that lead is "transparent" to neutrons, while its sensitivity to hydrogen enable resolving even fine details such as the leaf veins inside the flowers. Image credit: Daniel Hussey/NIST.

Materials/ Geological setting

This chapter will provide a short introduction to the samples that have been studied within the scope of this thesis, and brief description of the geological setting, where it is applicable. A detailed description of each sample can be found in the papers.

Paper I: The Mien impact structure

The studied samples in paper I were collected from the Mien impact structure (Fig. 7–8; 56.41812°N 14.85785°E). The structure is located in southern Sweden and is situated in the "Trans Scandinavian igneous belt", which stretches 1600 km from southeastern Sweden to northwestern Norway. The depression is today filled by a lake, and the island Ramsö (approximately in the center of the lake) has been interpreted to be a remnant from the central uplift and is also the only location in the immediate area of the lake where outcrops can be found (Åström 1998). The surrounding bedrock in the area consists of Precambrian (1.8–1.4 Ga) granites and gneisses, and the bottom of the lake is filled by glaciofluvial sediments from the last glaciation. The first geological report of the structure is from 1890 (Holst 1890), in which rocks, sampled from around the lake, were described as "abnormal magmatic rocks" that "look like incomplete molten products, made artificially". However, the elusive Mien impactites were noticed long before Holst published his report; findings of neolithic settlements in the area show that these rocks were chosen as material for stone axes (Nilsson 2003) and possibly favoured because of the peculiar terrain of Mien (Nilsson 2003).

Holst (1890) suggested that the structure could be a remnant of a tertiary volcano, but with some hesitation; he sent samples to the petrographer Prof. F. Zirkel, who wrote back (in a letter dated March 13, 1888), that "… I would not entirely reject the idea that a completely abnormal process is responsible for their genesis". At a meeting of the Geological Society of Stockholm, A. G. Högbom compared Mien to the newly confirmed Meteor Cra-

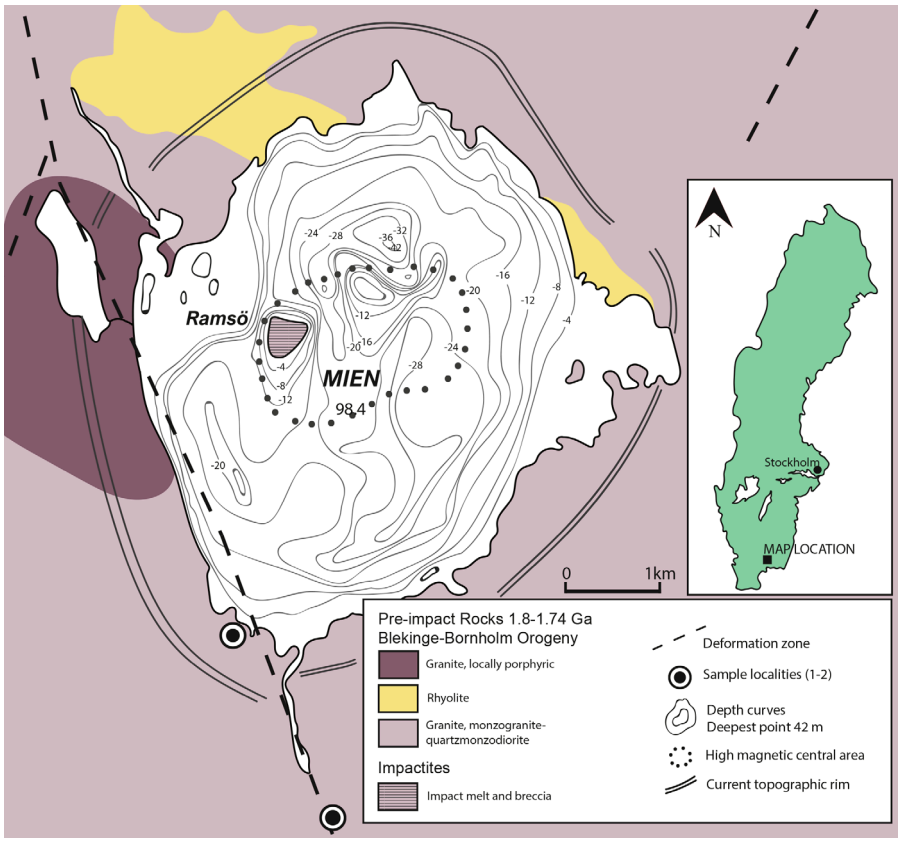

Figure 7. Geological map of the Mien impact structure (from Paper I). Sample localities for the impact melt rocks and the suevitic breccia are marked in the figure. Figure from Martell et al. 2021.

Figure 8. Photograph from the shore of Lake Mien. Ramsö island (remnant from the central uplift) is visible in the horizon. (Photo: Josefin Martell)

ter in Arizona and suggested a similar origin for both structures (Högbom 1910). It can also be noted that Holst, although he could not explain its formation, in his report actually provided the first drawing of ballen silica, which can be found in specific types of impactites, and that has a characteristic-looking texture consisting of ovoid aggregates that result from back-transformation from shock-induced states (Ferrière et al. 2010).

The similarity between certain rocks from Mien and suevite from the Ries impact structure in Germany was also noted relatively early; guided by known coesite-bearing samples from Ries, Svensson and Wickman (1965), were able to find coesite in Mien impactites, and together with evidence of PDFs in quartz (von Engelhardt and Stöffler 1965) it was soon more or less accepted that the Mien structure had an impact origin.

The structure has been dated to 121.0±2.3 Ma using ^{40}Ar–^{39}Ar (Bottomley et al. 1978) and later recalculated to 122.4±2.3 Ma using updated decay constants (Schmieder and Kring 2020). The current diameter of the lake is ~6.5 km, but its original diameter has been estimated to be 9 km (Åström 1998). Three drill cores from the lake were recovered in the 1970s, in which the first ~20 meters are impact melt rock, followed by a small horizon of melt-bearing breccia (the "Mien suevite") and brecciated target rock.

The samples used in Paper I consist of two impact melt rock samples with varying clast content (one being more clast rich than the other) and a sample of suevitic breccia (or melt-bearing breccia). The impact melt rocks samples have a glassy matrix and contain lath-like microlites of plagioclase and feldspar, ballen silica, and quartz with two sets of PDFs. The suevitic breccia is a polymict, porous breccia containing fragmented crystalline lithic clasts and melt particles in a fine-grained clastic matrix. The impactite samples were collected at the lake shore and in a gravel pit south of the lake, respectively (Fig. 7).

Paper II: Martian "nakhlite" meteorites

The nakhlite meteorites are igneous, pyroxene-rich rocks deriving from Mars. On the basis of their similar ejection age (~11 Ma), petrology, and geochemistry, they are thought to derive from the same source region (Nyquist et al. 2001; Treiman 2005). Their crystallization ages range between ~1416 to 1322 Ma and they were likely emplaced in at least four magmatic events (Cohen et al. 2017). Several nakhlites show evidence of pre-terrestrial aqueous alteration in the form of clay minerals, or "iddingsite" (e.g., Bunch and Reid 1975; Darby et al. 2005), cross-cutting mainly olivine grains of the samples. A Martian origin of the iddingsite has been determined by hydrogen isotopic systematics (Watson et al. 1994; Hallis et al. 2012), and by chemical and isotopic compositions that are consistent with in-situ analyses on Mars (Treiman 2005; Corrigan et al. 2015; Udry and Day 2018). A correlation between shock microstructures in augite and secondary mineral assemblages, suggest that the heat from an impact event facilitated the alteration (Daly et al. 2019a).

The source terrain of the nakhlites is not known, but suggestions include the large volcanic terrain of the northern plains, Tharsis, Elysium-Amazonis volcanic plains, and Syrtis Major (Bridges and Warren 2006; Bridges and Schwenzer 2012). In paper II, we show the results of combined NCT, XCT, and EBSD on two specimens of the Miller Range (MIL) 03346 meteorite. MIL 03346 is a nakhlite composed of phenocrystic clinopyroxene, with lesser amounts of olivine (crosscut by iddingsite) and skeletal Fe-Ti oxides, in a fine-grained mesostasis (Day et al. 2006a). The results from one of these specimens are also reported in Paper III.

Paper III: Case studies

Paper III includes results from four samples, presented as case studies: (1) a sample of Libyan des-

ert glass, (2) a Chicxulub drill core sample, (3) a Luizi impact melt rock sample, and (4) a specimen of the Martian MIL 03346 meteorite. MIL 03346 is described in the previous section (4.2).

Libyan desert glass

Libyan Desert Glass (LDG) is a silica-rich (98 wt. % SiO_2) impact glass found in the desert at the border between Libya and Egypt, and formed ~29 million years ago (Fig. 9). The glass occurs as centimeter to decimeter-sized pieces, with colors ranging from light yellow to light green. Some pieces contain characteristic, layering or "bands" of dark brown material, suggesting a flow structure (Fig. 9; e.g., Pratesi et al. 2002). These bands consist mainly of isolated spherules of Fe, Al, and Mg that have formed an emulsion with the silica glass as a result of silicate-silicate liquid immiscibility (Pratesi et al. 2002). Low osmium isotopic ratios (Koeberl 2000; Koeberl and Ferrière 2019), and enrichment of siderophile elements (e.g., Cipriani et al. 2000; Giuli et al. 2003) have indicated a the presence of a meteoritic component in the bands. Because of this, a sample of Libyan Desert Glass, containing dark banding, was investigated using NCT and XCT (Paper III), aiming to pinpoint projectile material. The impact origin of the glass has been confirmed by findings of the former presence of the impact diagnostic, $ZrSiO_4$ high-pressure polymorph reidite (FRIGN zircon; Cavosie and Koeberl 2019). No source crater has been identified and the nature of the target rock is under debate, although a recent study suggests a loose sedimentary formation with sandstones of different ages (Sighinolfi et al. 2020).

Figure 9. Map showing the approximate location where Libyan Desert Glass (LDG) samples have been found. In the lower right is the investigated sample in our study (Sample size is about 2 cm along the longest axis).

Chicxulub drill core sample

To date, the only hypervelocity impact that has been linked to a mass extinction is the one that marks the Cretaceous–Paleogene (K–Pg) boundary (Alvarez et al. 1980; Smit and Hertogen 1980; Schulte et al. 2010). The boundary is marked by a thin layer of clay containing elevated concentrations of iridium relative to continental crustal background levels, and has been found in the geological record across the globe (e.g., Kiessling and Alvarez 2002; Schulte et al. 2010). Besides iridium, the layer is enriched in other moderately (e.g., Ni, Co) and highly siderophile elements (Ru, Rh, Pd, Re, Os, Pt, and Au; e.g., Schulte et al. 2010). The impact resulted in a ~200 km-sized impact structure, located on the Yucatán Peninsula of Mexico (Hildebrand et al. 1991). In 2016, a continuous drill core from 505.7 to 1334.7 meters was recovered from the peak ring of the crater (International Ocean Discovery Program (IODP); Morgan et al. 2016; Goderis et al. 2021). The sample investigated in Paper III is from the IODP-ICDP Expedition 364 drill core sample 364_77_A_040_R_001_36.5-39.0 (recovered between 616.605 and 616.63 meters below sea floor; see e.g., Goderis et al. 2021). The interval represents a transitional unit mainly composed of brown-to-gray carbonate-rich claystone (Goderis et al. 2021). A sample of this particular unit was chosen for combined XCT/NCT because of elevated concentrations of Ir, Ni, Re, and Os concentrations compared to the upper continental crust (Goderis et al. 2021).

Luizi impact melt rock

The 17-km-wide Luizi impact structure is located in the Democratic Republic of the Congo (10°10'13.5"S / 28°00'27.0"E; Ferrière et al. 2011a) and is the first confirmed impact structure in Central Africa (Ferrière et al. 2011b). Findings of shatter cones, shocked quartz grains (Ferrière et al. 2011a), and the former presence of reidite in shocked zircon grains (Cavosie et al. 2018a) have confirmed an impact origin of the structure. The target rock is part

of the Kundelungu plateau, which consists of Neoproterozoic (~574 Ma) arkosic sandstones (Claeys et al. 2008) that are melted and deformed at the central peak of the structure (Cavosie et al. 2018b). The sample in Paper III derives from a boulder retrieved from a lake 6.2 km from the original crater center of the structure. The boulder is an impact melt rock that consists of acicular SiO_2 crystals in an aluminosilicate glass with quartz, alkali feldspar, biotite, and clinopyroxene (Cavosie et al. 2018a). Zircon, Fe-Ti oxides, and chromite occur as accessory phases (Cavosie et al. 2018a). The sample was included in this study to investigate whether it contains traces of projectile material as well as to explore if combined NCT and XCT could help in distinguishing between various features in this impactite lithology.

Summary of papers

The author's contribution to each paper is given in Table 1.

Paper I

Martell, J., Alwmark, C., Holm-Alwmark, S. and Lindgren, P. (2021), *Shock deformation in zircon grains from the Mien impact structure, Sweden.* Meteoritics & Planetary Science, *56*:362–378.

In this paper, we present the first detailed investigation of shock deformation in zircon grains from the Mien impact structure in Sweden. The zircon grains derive from two impactite lithologies: a suevitic breccia and two specimens of impact melt rock with varying clast content, of which petrographic descriptions of each sample are given. Ballen silica was found in the impact melt rock sample, and all samples contain quartz grains with planar deformation features (measured using a Universal stage). Shock textures in zircon grains were identified using EBSD and the results show that several zircon grains with granular textures display a systematic misorientation between granules, which is indicative of the former presence of the zircon high-pressure polymorph reidite ("FRIGN" zircon). Reidite forms at shock pressures of ~30 GPa in crystalline targets, and is only known from impact structures. A majority of the zircon grains also display granular and/or "microporous" textures that we relate to the impact (although not diagnostic). Recognition of shock metamorphic features is crucial for confirming impact structures. Our study shows that impact-diagnostic FRIGN zircon can be expected also from relatively small impact structures, with little material available due to e.g., erosion. We conclude with a recommendation that zircon grains from the impact melt rock could be targeted for a refined age dating of Mien.

Paper II

Martell J., Alwmark C., Daly L., Hall S., Alwmark S., Woracek R., Helfen L., Hektor J., Tengattini A., Lee M. 2022. *The scale of a hydrothermal system explored using combined neutron and x-ray tomography.* Science Advances, *8*(19), eabn3044.

In this paper we used combined neutron– and X-ray tomography, together with SEM-EBSD techniques, to investigate the 3D distribution of hydrous alteration (iddingsite) in two nakhlite meteorite specimens: Miller range (MIL) 03346,231 and MIL 03346,230. Previous studies have shown that the iddingsite formed from pre-terrestrial hydrous alteration, and that the alteration event likely took place ~650 Ma, i.e., after the crystallization of the sample (~1.3 Ga). The iddingsite often occurs in association with shock deformation, which suggests that the ingress of fluids was facilitated by shock fracturing following a meteorite impact. If large enough, an impact-induced hydrothermal system could retain heat and moisture for millions of years and might be a favorable environment for microbial life. We, therefore, set out to explore the scale of the hydrothermal system, by pin-pointing the iddingsite in three dimensions. Our results show that the aqueous phases mainly cluster around olivine grains, with limited interconnectivity between clusters. These results indicate that the alteration event was likely short, and that a potential fluid source could be local patches of sub-surface ice that melted during a heat pulse from an impact event, or that the location where the sample was sourced was in the vicinity of the hydrothermal system. Furthermore, the results also highlight the advantages of using non-destructive methods, in particular neutron tomography, in studies of meteorites.

Paper III

J. Martell, C. Alwmark, R. Woracek, S. Alwmark, S. Hall, L. Ferrière, C. Daly, L., Bender Koch, J. Hektor, L. Helfen, A. Tengattini, D. Mannes. *Combined neutron and x-ray imaging for detecting projectile material and hydrous constituents in meteorites and terrestrial impactites.* Manuscript.

In this "proof-of-concept" study we show results from combined neutron- and X-ray tomography (NCT/XCT) of four different impactite samples. Our primary aim was to demonstrate that these methods can be used to locate projectile material in impactite samples, but also to show the capabilities of combined XCT/NCT/EBSD for investigating other features in planetary samples. The investigated samples are: a sample of Libyan Desert glass (LDG); an impact melt rock sample from the Luizi impact structure; a Chicxulub drill core sample; and a sample of the Martian meteorite MIL 03346. Two samples (LDG and the Chicxulub drill core) were chosen because of previous studies showing the presence of a meteoritic component. Using both methods, we were able to pin-point a FeNi silicide spherule in the impact glass. However, we did not detect projectile material in the Chicxulub drill core sample; this could be due to poor resolution or too little available projectile material in this specific sample, or that the hydrogen-rich clay obscures other features. Nevertheless, the LDG spherule shows that projectile material can be detected using combined NCT and XCT. The impact melt sample was scanned with the aim of evaluating how combined NCT and XCT can help distinguish between different minerals; using both methods, it was possible to both segment clay (based on NCT images), zircon grains, and two spherical "rims" of iron oxides (based on XCT images). These results highlight the complementarity of the methods. The Martian meteorite was included to demonstrate that NCT is outstanding in locating hydrous phases, which would be interesting for other meteorites as well. We also discuss limitations using XCT/NCT when studying planetary samples and how these can be addressed, and implications for future sample return missions. To conclude, we share our expertise on these methods, providing a "recipe" for other researchers that want to pursue studies using these techniques.

Table 1. Author contributions.

	Paper I	Paper II	Paper III
Study design	**J. Martell**	C. Alwmark	**J. Martell**
	C. Alwmark	L. Daly	C. Alwmark
	S. Alwmark	R. Woracek	S. Alwmark
	P. Lindgren		
Data collection			
Field work/Sampling	**J. Martell**		
	C. Alwmark		
Sample preparation for SEM-EBSD	**J. Martell**	**J. Martell**	**J. Martell**
			C. Alwmark
Neutron tomography		S. Hall	L. Helfen
		L. Helfen	A. Tengattini
		A. Tengattini	S. Hall
		J. Martell	R. Woracek
			D. Mannes
			J. Martell
X-ray tomography		S. Hall	S. Hall
SEM-EBSD	**J. Martell**	**J. Martell**	**J. Martell**
	C. Alwmark	C. Alwmark	C. Alwmark
Data analysis			
Registration of tomography data		**J. Martell**	**J. Martell**
		J. Hektor	
Data interpretation	All authors	**J. Martell**	**J. Martell**
		C. Alwmark	C. Alwmark
		L. Daly	S. Alwmark
		R. Woracek	R. Woracek
		S. Alwmark	S. Alwmark
		S. Hall	
		J. Hektor	
Figures and illustrations	**J. Martell**	**J. Martell**	**J. Martell**
Writing: original draft	**J. Martell**	**J. Martell**	**J. Martell**
Writing: review and editing	All authors	All authors	All authors

Discussion of results

This overall motivation with this thesis was to explore, and pave the way for, how advanced imaging techniques can be used to study impactites, either as an alternative to more "conventional" imaging techniques, or as a complementary method, to maximize the scientific outcome.

In *Paper I*, we showed that zircon within impact melt samples from the Mien impact structure contain evidence of the former presence of reidite (FRIGN zircon), highlighting the diversity of shock pressures recorded by shocked materials in the samples, which allowed us to give a pressure estimate of at least 30 GPa for these grains. In *Paper II*, we showed that combined neutron- and X-ray tomography can be used to render the distribution of hydrous phases in Martian meteorites in 3D, and discussed implications for the Martian meteorite MIL 03346. In *Paper III*, we show that combined XCT/NCT can be used to locate projectile material in impactite samples.

Shocked zircon from the Mien impact structure

In this paper, we present the first finding of FRIGN (former reidite in granular neoblasts) zircon from a Swedish impact structure. Shocked zircon grains were found in two impactite lithologies: impact melt rock and suevitic breccia. We also include documentation of other microtextures in both zircon- and quartz grains that we relate to the impact event.

The target rock at the Mien impact was crystalline, and shock experiments have shown that the formation of reidite takes place at pressures of ~30 GPa in crystalline rocks (Kusaba et al. 1985; Leroux et al. 1999) and that the transformation is complete at pressures of ~50 GPa. The reversion back to reidite occurs at temperatures >1200°C (Kusaba et al. 1985; Fiske 1999). Several FRIGN zircon grains from the Mien impactites also contained micrometer-sized inclusions of ZrO_2, indicating that the granular texture formed at temperatures in excess of 1673°C, which is when zircon begins to dissociate (e.g., Kaiser et al. 2008). FRIGN zircon with ZrO_2 inclusions thus both records the high pressures needed to form reidite, and the high temperatures required both for reidite to revert back to zircon, and for zircon to dissociate into ZrO_2. (Cavosie et al. 2018a). However, it should be mentioned that the target lithology affects the shock response of zircon; recent shock experiments showed that reidite starts forming at pressures from 10 to 17.5 GPa in sedimentary target rocks, likely as the result of the pore-space leading to localized shock pressure amplification (e.g., Bishop 2022; Cavosie et al. 2022). Furthermore, pre-impact radiation damage might also influence whether the zircon grain will transform into reidite or not (Erickson et al. 2017). Although the exact (pressure) number might change slightly over time, our study shows that FRIGN zircon can be expected also from relatively small and eroded hypervelocity impact structures, with little material available, expanding the type of setting where it has been described. Shock-recrystallized zircon has also successfully been used to provide ages for impact events, e.g., (e.g., Kenny et al. 2017; Erickson et al. 2020), making the granular grains from Mien prime candidates for refining the age of the Mien impact, and the results from Paper I resulted in a follow-up study by Herrmann et al. 2022 (currently in review; manuscript not included in this thesis).

The terminology of the Mien impactites has varied over time; the impact melt rock is sometimes referred to as "Mien rhyolite" (e.g., Holst 1890; Ekelund and Ekström 1990) or Mienite (Henkel 1992), which might have contributed to that the, since the 1970s, obsolete theory of a volcanic origin of Mien, still is mentioned as a possibility on the information signs around the lake. Furthermore, when the structure was mentioned in Swedish state media (SVT) in 2007, the news article was accompanied by a fact box describing the formation of rhyolite (which was correct, if it had been a rhyolite). There is also an on-going discussion on the formation of "suevites" (Osinski and Grieve 2017), why we recommend using the term suevitic breccia (according to the classification by Stöffler et al. 2018) or melt-bearing breccia for this rock type.

To conclude, we did consider including complementary XCT of Mien zircon grains; a 3D characterization of the exterior of detrital zircon grains from the Murchison River has previously been done by Markwitz et al. (2017), with the aim of quantifying how fluvial transport affects the 3D shape. They obtained a voxel resolution of 5.14 µm, which would be sufficient for a simple 3D rendering

of the exterior of the Mien zircon, but would likely not provide any insights to the shock metamorphic features observed using SEM-EBSD. Suuronen and Sayab (2018) attempted a multimodal X-ray nanotomography approach (X-ray absorption, diffraction, and fluorescence tomography) to quantify internal structures in zircon grains from the Central Finland Granitoid Complex, and were able to identify and segment 1–5 µm-sized inclusions within the zircon grains as well as internal fractures. A similar study could potentially be interesting for shocked zircon but would expand the project significantly. Due to the many lock downs of research facilities and departments half-way through the thesis work and the subsequent delays of the other studies (Paper II and III) we decided that the EBSD results could be published without the addition of more techniques. For a future study, it could be interesting to make an attempt at X-ray nanotomography of shocked minerals, to get insight into e.g., the distribution of microfractures and possibly other microtextures. Furthermore, an initial XCT and/or NCT scan of the impactite sample could guide what regions to target for obtaining highly shocked material, e.g., to locate zircon grains for geochronological purposes.

Combined NCT and XCT imaging of planetary samples

Paper II and III show that utilizing several different imaging methods, starting with the least destructive (NCT and XCT), followed by more destructive (SEM-EDS/EBSD) ones, can provide insights into planetary samples that would not have been possible by using only one technique. NCT is particularly suitable for investigating hydrous alteration in meteorites, but the XCT images were crucial for characterizing other phases in the MIL 03346 sample.The tomography images also "save" information for future studies, even if the sample has been sectioned or consumed using destructive methods. This may be especially important for rare and delicate samples, such as specific meteorite types or returned samples (e.g., Tsuchiyama et al. 2002). Tomography can also be employed to avoid sample bias, for example, if only a small amount of material is allowed to be sectioned. Comparing thin sections to the 3D images can thus strengthen any interpretation made.

Insights into Martian meteorites using combined NCT and XCT

Paper II focused on the nakhlite MIL 03346, which is known to contain pre-terrestrial alteration assemblages in the form of iddingsite (e.g., Treiman 2005; Day et al. 2006b; Hallis and Taylor 2011; Hallis et al. 2012). The nakhlites are believed to have been emplaced in the same source region (Udry and Day 2018) and have similar crystallization ages and ejection ages (e.g., Nyquist et al. 2001; Cohen et al. 2017). MIL 03346 was likely emplaced close to the ground surface, indicated by a fine-grained mesostasis and the absence of feldspar (Hallis and Taylor 2011). Several authors have proposed that the aqueous alteration could have been facilitated by an impact event, which could both fracture the rock and melt sub-surface ice, such as permafrost (Changela and Bridges 2010; Daly et al. 2019a). With our study, we wanted to explore the distribution of the hydrous alteration to see whether it is pervasive throughout the sample or if it occurs as patches, which could give insights into the source of the fluids and the longevity of the (potential) hydrothermal system. The 3D images show that the iddingsite occurs as discrete "clusters" within and around the olivine grains, and occasionally as localized patches in the mesostasis, but with limited interconnectivity between the clusters (Fig. 10). Furthermore, the EBSD analysis revealed shock deformation in augite grains in the altered areas. The findings support that a fluid source could be localized patches of sub-surface ice, which melted during an impact event. A limitation to this type of study is the small amount of material investigated, as well as the lack of a geological context. Using these techniques on other nakhlites could possibly shed light on the differences between the samples, for example, if they are altered to the same extent; e.g., based on higher water rock ratios in rocks excavated from greater depths, it could be expected that these are more heavily altered. This study also highlights that comparative investigations of this sort can be interesting for future sample returns, such as the Mars sample return campaign.

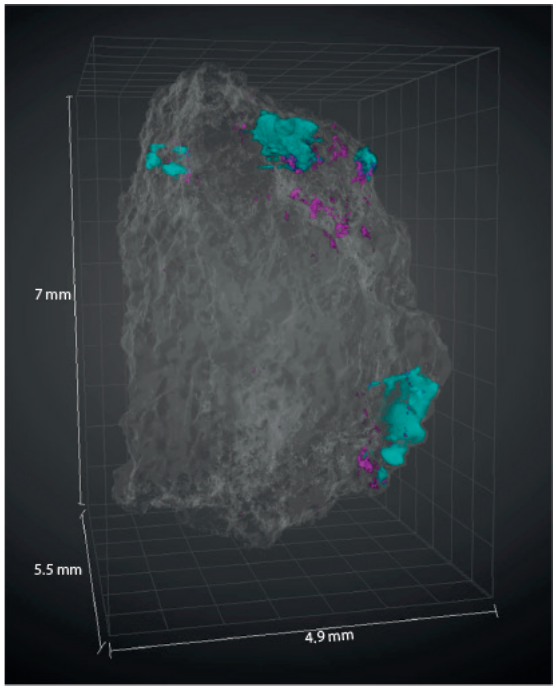

Figure 10. 3D rendering of MIL 03346, based on segmented phases from both the X-ray and the neutron images. Olivine grains are segmented in cyan, and the hydrous phases in magenta. The results show that the hydrous phases mainly are clustered within and around the olivine grains. Figure from Martell et al. 2022 (Paper II).

Combined XCT and NCT for locating projectile material

An intriguing opportunity with NCT and XCT is that both modalities have a high iridium attenuation. Combining these methods, and only investigating inclusions with both high X-ray and high neutron attenuation, thus opens up the possibility to locate projectile material, such as PGE-nuggets in impactites, which is today usually done by employing whole-rock techniques. We decided to scan two samples with a known projectile component; a sample from the Chicxulub drill core, and a sample of Libyan Desert Glass (LDG). By comparing the 3D images slice-by-slice we were able to locate an inclusion in the LDG with high attenuation for both modalities (Fig. 11). The sample was carefully polished to enable detailed investigation of the inclusion, and the SEM-EDS analysis revealed it to be a 80 µm-sized FeNi silicide spherule. These have not been found in the LDG before. However, Hamann et al. (2022) reported nanometer-sized FeNi silicides from the Wabar impact glass, and interpreted those as mixtures of impact-vapor condensates mixed with condensates from the ablation of the impactor. Combined NCT and XCT is thus a promising technique for studies of other impact glasses, which ultimately could provide insight into processes in the impact plume. The EDS map of the spherule did not show a presence of PGEs, but we will conduct further analyses (higher resolution XCT, and possibly Inductively coupled plasma mass spectrometry) to better constrain its origin. The K–Pg sample seemed to be the most promising sample for this study due to a known PGE contribution in this specific interval. However, we did not detect any potential PGE-rich inclusions in the K–Pg sample; the reason could be that the hydrogen-rich clay "overshadows" other phases, a too low resolution of the 3D images, or that this particular specimen does not contain high amounts of PGEs.

Using combined NCT and XCT to locate projectile material involves several steps; from selecting the sample, to applying to beam time, processing and analysis of 3D images, and preparing for SEM analysis by polishing the sample (Fig. 11). If potential projectile material is found, it then has to be further investigated using e.g., isotopic analyses (e.g., Koeberl 1998; Goderis et al. 2012b). It is therefore crucial to establish what works, and what does not. It is still relatively difficult to get access to neutron facilities, and it is both important to motivate the need for beamtime and to use the allocated time efficiently. By showing the results of combined XCT and NCT on several different impactite samples, the intention is to provide some guidance into what samples that may yield the most promising results.

Conclusions and outlook

Compared to XCT, NCT is still an unexplored imaging technique in planetary science, but will most likely find new users and applications in the up-coming years; the neutron facility European Spallation source (ESS) is currently being built in Sweden, and will open to users in the near future. XCT will be employed early in the analyses pipeline for the Mars Sample Return (e.g., Welzenbach et al. 2017; Tait et al. 2022). For NCT to be considered alongside XCT, it will be crucial to determine how neutrons affect samples on a sub-µm scale, especially organic compounds. Although both methods are considered non-destructive, the interaction between the neutrons/X-rays and the sample material can affect e.g., isotopic systems (Sears et al. 2016; Treiman

et al. 2022). Furthermore, it is worth keeping in mind that what is undetectable today might not be in the future, and plan the experiments accordingly.

Nevertheless, we conclude that NCT is a powerful method for locating hydrous material and projectile components within rocks without having to cut them open, and that XCT and NCT will be key techniques in future studies of planetary materials.

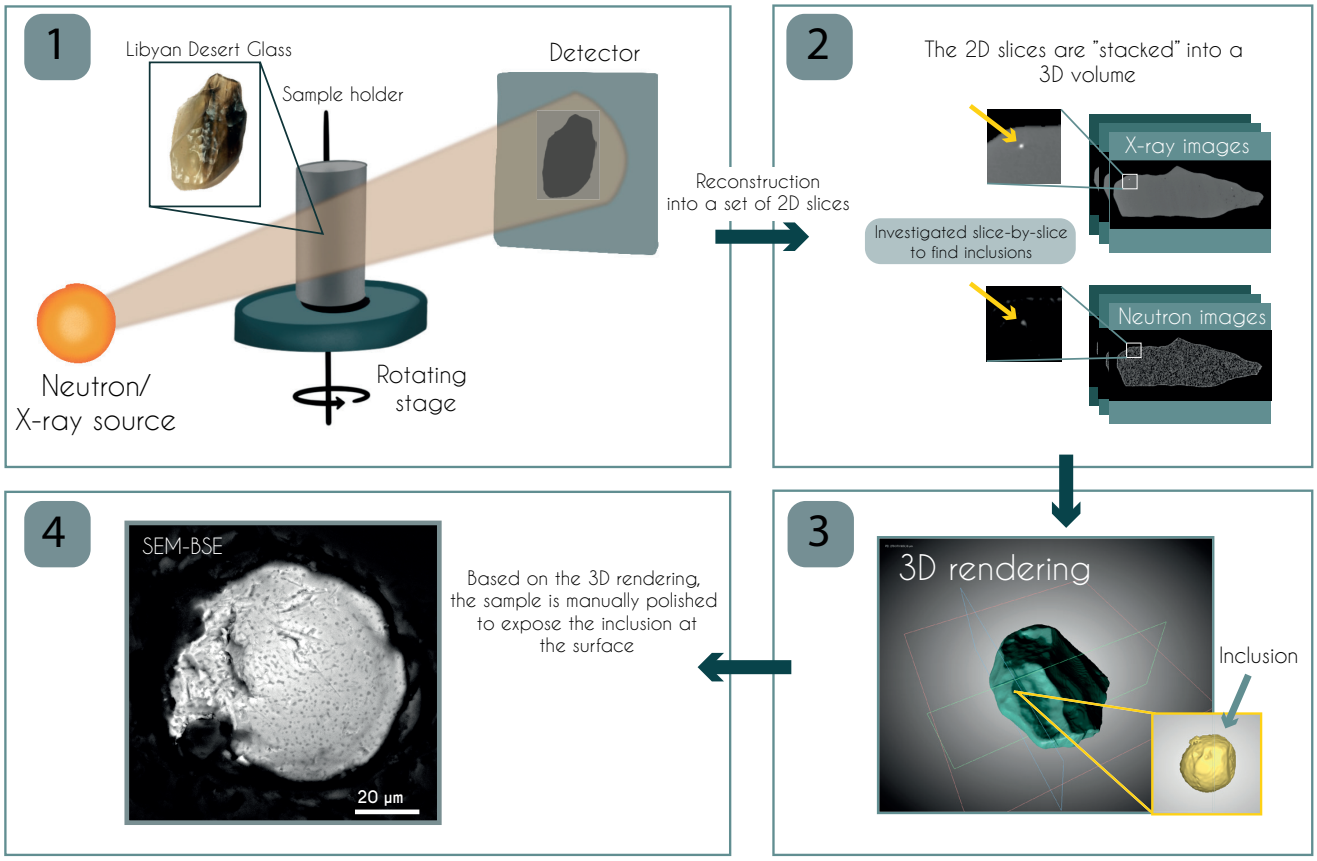

Figure 11. Method used to locate projectile material using combined NCT and XCT. 1: The setup for XCT and NCT is similar; the sample is placed in a sample holder that is mounted on a rotating stage. A detector measures the decrease in intensity between the incident beam and the final beam, after traversing the sample. 2: The tomograms are reconstructed into 2D slices that are then stacked so that they can be viewed as a 3D volume. The two data sets (NCT and XCT) are "registered" (aligned) so that they can be compared slice-by-slice. For projectile detection, regions-of-interest are inclusions that are highly attenuating for both modalities. 3: If an inclusion is found, it can be rendered in 3D and located within the volume. 4: The sample is manually polished to expose the inclusion at the surface for e.g., SEM analysis.

Populärvetenskaplig sammanfattning

Av alla geologiska strukturer på stenplaneterna (och månarna) i vårt solsystem så är nedslagskratrar den vanligaste. Detta är kanske oväntat eftersom vi har förhållandevis få på jorden – det räcker att se upp på vår egen måne för att få en uppfattning om hur jorden hade kunnat se ut, eftersom det varit precis lika många meteoritnedslag på jorden som på alla andra steniga himlakroppar. Bevarandegraden på jorden är dock väldigt dålig: plattektonik, erosionsprocesser, samt hav och vegetation som täcker stora delar av jordytan gör att få nedslagskratrar, eller nedslagsstrukturer eftersom själva kratern sällan finns kvar i sin ursprungliga form, från jordens tidiga historia finns bevarade – den äldsta som vi känner till är ”endast” 2.2 miljarder år gammal (Yarrabubbastrukturen i Australien).

Vi kan studera vad som händer vid dessa nedslag genom att undersöka de bergarter som bildats eller modifierats vid nedslaget, s k impaktiter. De extrema tryck och temperaturer som uppstår vid meteoritnedslag uppgår till 1000 gigapascal (inne i jordens kärna är det cirka 380 gigapascal) och sker på en mikrosekund från det att projektilen, dvs det som kolliderar med jorden, når jordytan. Chockvågen som genereras deformerar bergarter och mineral på ett vis som är unikt för nedslagsprocessen, s k chockmetamorfos. Det mesta av själva projektilen förångas, men lite material från den kan mixas med den uppsmälta berggrunden. I ett av projekten i denna avhandling letar vi efter dessa spår av projektilen, genom att analysera impaktiter. Vanligtvis så krossar eller upplöser man impaktiterna och analyserar allt pulver på samma gång. Målet i vår studie är att istället först lokalisera projektilmaterial i 3D, för att sedan kunna extrahera för mer detaljerade analyser, vilket minskar risken för att missa material, bevarar kontext (hur förhåller sig projektilmaterialet till andra mineral i impaktiten?), och ge insikt i vad som händer kemiskt när projektilmaterial blandas med den uppsmälta berggrunden. Våra resultat visade att kombinerad röntgen- och neutrontomografi kan användas för detta ändamål. Vi hittade nämligen en järn-nickel-inklusion som förmodas innehålla projektilmaterial. Vi beskriver i manuskriptet hur denna metod fungerar, och diskuterar begränsningar och möjligheter med de icke-destruktiva teknikerna röntgen- och neutrontomografi.

Vi har även undersökt impaktiter från sjön Mien, som är en nedslagsstruktur vid gränsen mellan Blekinge och Småland. Impaktiterna krossades till ett fint pulver för att zirkon skulle kunna separeras ut. Detta gjordes sedan under mikroskop med hjälp av ett penselstrå (!), eftersom zirkonkornen inte är större än cirka 50 µm, vilket är ungefär som tjockleken av ett hårstrå. Dessa korn studeras sedan med ett svepelektronmikroskop. När berggrunden utsätts för chockmetamorfos, så kan vissa mineral ”omvandlas” till högtrycksfaser (eller ”polymorfer”), ungefär som grafit och diamant som har samma kemiska sammansättning men olika kristallstruktur. Dessa högtrycksfaser är inte stabila vid trycket uppe vid jordytan, och kommer i vissa fall tillbakabildas till sitt ursprungsmineral. När vi undersökte zirkonkorn från Mien kunde vi se att vissa av dem tillbakabildats från högtrycksfasen reidite; reidite är indikativt för nedslagsprocesser, och bildas vid ungefär 30 gigapascal. Detta tryck motsvarar trycket som råder nästa 1000 km ned under jordytan. Fördelen med att hitta dessa material är att de både kan lära oss om själva nedslaget, t ex vilka tryck och temperaturer som råder på olika platser i en krater, men också att de kan användas för att bevisa att en struktur bildats av ett nedslag och inte av någon annan geologisk process. Zirkon har också en annan fördel, nämligen att de rutinmässigt används för att datera berggrunden. En slutsats är att de zirkoner vi funnits skulle kunna användas för att ge en mer korrekt datering av Mien-nedslaget.

Vi har även undersökt en meteorit från Mars med syftet att förstå hur vatten rört sig genom provet. Just denna meteorit har nämligen reagerat med flytande vatten vid något tillfälle när det fortfarande var del av berggrunden på Mars; detta kan man se på t ex mineralet olivin, som i sprickor omvandlats till olika slags lermineral. Man har räknat ut lermineralen bildades för ungefär 600 miljoner år sedan. Detta var långt efter att meteoriten först kristalliserade (cirka 1.3 miljarder år sedan) och under en ”torr” period på Mars, då man tror att allt flytande vatten försvunnit från Marsytan. Vi ville därför ta redan på hur mycket vatten som rört sig genom meteoriten; om det fanns mycket vatten tillgängligt vid denna tidpunkt så skulle det nämligen kunna vara en gynnsam miljö för mikrober. Vi använde oss av rönt-

gen- och neutrontomografi, och våra resultat visade att lermineralen bildade kluster runt olivinkornen, men att dessa inte såg ut att vara sammankopplade, till exempel genom spricksystem. Detta tyder dels på att själva källan till vattnet måste varit lokal, samt att det inte skulle vara en gynnsam miljö för mikrobiellt liv. Vår tolkning är att det funnits lokala ansamlingar av underjordisk is (permafrost) som smält upp och omvandlat olivinkornen, förmodligen i samman-band med ett meteoritnedslag.Neutrontomografi är en särskilt bra metod för att undersöka vatten (H_2O) i meteoriter och impaktiter; neutroner är nämligen väldigt känsliga för väte (H).

Sammantaget, så har vi med hjälp av avancerade ”imaging”-tekniker kunnat visa att neutron- och röntgentomografi kan användas för att lokalisera både väte och projektilmaterial i impaktiter. Vidare så föreslår vi att dessa metoder bör användas vid analys av material som hämtats från platser utanför jorden (exempel på material som “hämtats” från andra himlakroppar är t ex månproverna efter Apollo-expeditionerna på 1960- och 1970talet). Runt år 2030 så förväntas NASA hämta hem prover från Mars, och dessa kommer vara ovärderliga. Icke-destruktiva metoder kan därför vara till stor hjälp, både för att bedöma var destruktiva analyser ska göras för att spara så mycket material som möjligt, men också för att kunna göra analyser utan att förstöra provet.

Manuscripts and extended conference abstracts not included in this thesis

Herrmann, M., Kenny, G., Martell, J., Alwmark, C., Whitehouse, M. J. (2022). *First U–Pb age of shocked zircon for the Mien impact structure, Sweden, and implications for metamictization-induced zircon texture formation during impact events.* Manuscript in review in Meteoritics and Planetary Science.

Alwmark S. Alwmark C. Ferrière L. Martell J. Rae A. S. P. Zachén G. (2022). *Impact Crater Formation: Insights from >6,500 Meters of Shock Attenuation in the Central Uplift of the Siljan Impact Structure, Sweden.* 85th Annual Meeting of The Meteoritical Society. Abstract #6237.

Martell, J., Alwmark, C., Alwmark, S., Hall, S., Hektor, J., Woracek, R., Helfen, L., Tengattini, A. (2021). *Neutron tomography as a tool for pin-pointing meteoritic components in impactites.* 52nd Lunar and Planetary Science Conference. Abstract #2086.

Herrmann, M., Martell., J., Alwmark, C., and Whitehouse, M. J., (2019). *SIMS U-Pb dating and EBSD structural analyses of granular zircon from the Mien impact structure, Sweden.* Large Meteorite Impacts and Planetary Evolution VI. Abstract #5022.

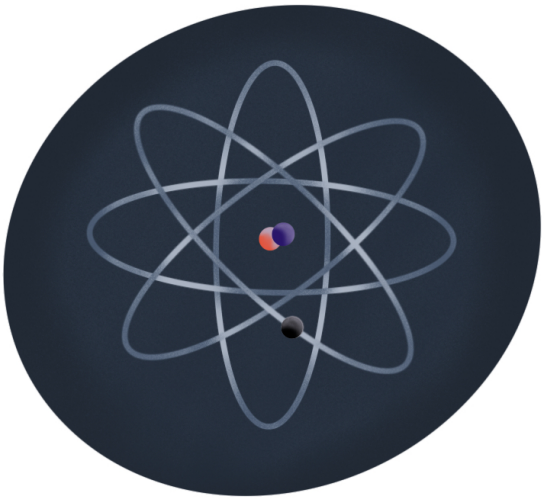

References

Abramov O. and Kring D. A. 2005. Impact-induced hydrothermal activity on early Mars. *Journal of Geophysical Research: Planets* 110.

Alvarez L. W., Alvarez, Walter, Asaro F., and Michel H. V. 1980. Extraterrestrial Cause for the Cretaceous-Tertiary Extinction. *Science* 208:1095–1108.

Alwmark C., Schmitz B., Holm S., Marone F., and Stampanoni M. 2011. A 3-D study of mineral inclusions in chromite from ordinary chondrites using synchrotron radiation X-ray tomographic microscopy—Method and applications. *Meteoritics & Planetary Science* 46:1071–1081.

Ames D. E., Watkinson D. H., and Parrish R. R. 1998. Dating of a regional hydrothermal system induced by the 1850 Ma Sudbury impact event. *Geology* 26:447–450.

Baker D. M. H., Head J. W., Collins G. S., and Potter R. W. K. 2016. The formation of peak-ring basins: Working hypotheses and path forward in using observations to constrain models of impact-basin formation. *Icarus* 273:146–163.

Barringer D. M. 1905. Coon Mountain and Its Crater. *Proceedings of the Academy of Natural Sciences of Philadelphia* 57:861–886.

Bishop J. 2022. Microstructural response of zircon in High-Porosity Seeberger Sandstone. Experimentally shocked from 2.5 to 17.5 GPa. Master of science, School of Earth and Planetary Science, Curtin University, Australia.

Blumenfeld E. J., Evans C. A., Oshel E. R., Liddle D. A., Beaulieu K., Zeigler R., Hanna R. D., and Ketcham R. A. 2015. Comprehensive non-destructive conservation documentation of lunar samples using high-resolution 3D reconstructions and X-ray CT data. 46th Lunar and Planetary Science Conference.

Bohor B. F. 1990. Shocked quartz and more; Impact signatures in Cretaceous/Tertiary boundary clays. In *Global Catastrophes in Earth History; An Interdisciplinary Conference on Impacts, Volcanism, and Mass Mortality*, edited by V. L. Sharpton and P. D. Ward, Geological Society of America.

Bohor B. F., Betterton W. J., and Krogh T. E. 1993. Impact-shocked zircons; discovery of shock-induced textures reflecting increasing degrees of shock metamorphism. *Earth and Planetary Science Letters* 119:419–424.

Bottomley R. J., York D., and Grieve R. A. F. 1978. 40Ar-39Ar ages of Scandinavian impact structures: I Mien and Siljan. *Contributions to Mineralogy and Petrology* 68:79–84.

Brenizer J. S. 2013. A Review of Significant Advances in Neutron Imaging from Conception to the Present. *Physics Procedia* 43:10–20.

Bridges J. C., Catling D. C., Saxton J. M., Swindle T. D., Lyon I. C., and Grady M. M. 2001. Alteration Assemblages in Martian Meteorites: Implications for Near-Surface Processes. *Space Science Reviews* 96:365–392.

Bridges J. C. and Warren P. H. 2006. The SNC meteorites: basaltic igneous processes on Mars. *Journal of the Geological Society* 163:229–251.

Bridges J. C. and Schwenzer S. P. 2012. The nakhlite hydrothermal brine on Mars. *Earth and Planetary Science Letters* 359–360:117–123.

Bunch T. E. and Reid A. M. 1975. The nakhlites Part I: Petrography and mineral chemistry. *Meteoritics* 10:303–315.

Cannon W. F., Schulz K. J., Horton Jr J. W., and

King D. A. 2010. The Sudbury impact layer in the paleoproterozoiciron ranges of northern Michigan, USA. *Geological Society of America Bulletin* 122:50–75.

Caporali S., Grazzi F., Salvemini F., Garbe U., Peetermans S., and Pratesi G. 2016. Structural Characterization of Iron Meteorites through Neutron Tomography. *Minerals* 6:14.

Carter N. L. 1965. Basal quartz deformation lamellae; a criterion for recognition of impactites. *American Journal of Science* 263:786–806.

Cavosie A. J., Erickson T. M., and Timms N. E. 2015. Nanoscale records of ancient shock deformation: Reidite (ZrSiO4) in sandstone at the Ordovician Rock Elm impact crater. *Geology* 43:315–318.

Cavosie A. J., Timms N. E., Ferrière L., and Rochette P. 2018a. FRIGN zircon—The only terrestrial mineral diagnostic of high-pressure and high-temperature shock deformation. *Geology* 46:891–894.

Cavosie A. J., Timms N. E., Ferrière L., and Rochette P. 2018b. Former Reidite in Granular Neoblastic Zircon (FRIGN Zircon) from the Luizi Impact Structure and Proposed Pantasma Structure. 49th Lunar and Planetary Science Conference.

Cavosie A. J. and Koeberl C. 2019. Overestimation of threat from 100 Mt–class airbursts? High-pressure evidence from zircon in Libyan Desert Glass. *Geology* 47:609–612.

Cavosie A. J., Biren M. B., Hodges K. V., Wartho J.-A., Horton J. W., Jr., and Koeberl C. 2020. Dendritic reidite from the Chesapeake Bay impact horizon, Ocean Drilling Program Site 1073 (offshore northeastern USA): A fingerprint of distal ejecta? *Geology*.

Cavosie A. J., Bishop J., Timms N., Reimold W., and Schmitt R. T. 2022. Experimental constraints on progressive shock deformation of zircon in porous target rocks shocked to pressures between 2.5 and 17.5 GPa. 85th Annual Meeting of The Meteoritical Society.

Chadwick J. 1932. The existence of a neutron. *Proceedings of the Royal Society of London. Series A* 136:692–708.

Changela H. G. and Bridges J. C. 2010. Alteration assemblages in the nakhlites: Variation with depth on Mars. *Meteoritics & Planetary Science* 45:1847–1867.

Chao E. C. T., Shoemaker E. M., and Madsen B. M. 1960. First Natural Occurrence of Coesite. *Science* 132:220–222.

Cipriani C., Corazza M., Giuli G., Moggi Cecchi V., Pratesi G., Rossi P., and Vittone E. 2000. Ion beam study of a possible extraterrestrial body signature in Libyan desert glass. *Nuclear Instruments and Methods in Physics Research Section B: Beam Interactions with Materials and Atoms* 170:187–192.

Claeys P., Chan J., and Dujardin R. 2008. The Luizi Structure: Remote Sensing Study of a Possible Impact Crater in Central Africa.

Cockell C., Osinski G., and Lee P. 2003. The Impact Crater as a Habitat: Effects of Impact Processing of Target Materials. *Astrobiology* 3:181–191.

Cockell C. S. 2004. Impact-shocked rocks – insights into archean and extraterrestrial microbial habitats (and sites for prebiotic chemistry?). *Advances in Space Research* 33:1231–1235.

Cockell C. S. 2006. The origin and emergence of life under impact bombardment. Philosophical Transactions of the Royal Society B: Biological Sciences 361:1845-1856

Cohen B. E., Mark D. F., Cassata W. S., Lee M. R., Tomkinson T., and Smith C. L. 2017. Taking the pulse of Mars via dating of a plume-fed volcano. *Nature Communications* 8:640.

Corrigan C. M., Velbel M. A., and Vicenzi E. P. 2015. Modal abundances of pyroxene,

olivine, and mesostasis in nakhlites; heterogeneity, variation, and implications for nakhlite emplacement. *Meteoritics & Planetary Science* 50:1497–1511.

Daly L., Lee M. R., Piazolo S., Griffin S., Bazargan M., Campanale F., Chung P., Cohen B. E., Pickersgill A. E., Hallis L. J., Trimby P. W., Baumgartner R., Forman L. V., and Benedix G. K. 2019a. Boom boom pow: Shock-facilitated aqueous alteration and evidence for two shock events in the Martian nakhlite meteorites. *Science Advances* 5:eaaw5549.

Daly L., Piazolo S., Lee M. R., Griffin S., Chung P., Campanale F., Cohen B. E., Hallis L. J., Trimby P. W., Baumgartner R., Forman L. V., and Benedix G. K. 2019b. Understanding the emplacement of Martian volcanic rocks using petrofabrics of the nakhlite meteorites. *Earth and Planetary Science Letters* 520:220–230.

Darby D. M., H. T. A., M. P. C., Takahiro H., D. L. M., and Vanessa O. C. 2005. MIL03346, the most oxidized Martian meteorite: A first look at spectroscopy, petrography, and mineral chemistry. *Journal of Geophysical Research: Planets* 110.

Day J. M. D., Taylor L. A., Floss C., and McSween H. Y. 2006a. Petrology and chemistry of MIL 03346 and its significance in understanding the petrogenesis of nakhlites on Mars. 41:581–606.

Day J. M. D., Taylor L. A., Floss C., and McSween Jr H. Y. 2006b. Petrology and chemistry of MIL 03346 and its significance in understanding the petrogenesis of nakhlites on Mars. *Meteoritics and Planetary Science* 41:581–606.

Dragonfly 2021.1 [Computer software] 2021. Object Research Systems (ORS) Inc, Montreal, Canada.

Dressler B. O., Sharpton V. L., and Schuraytz B. C. 1998. Shock metamorphism and shock barometry at a complex impact structure: Slate Islands, Canada. *Contrib Mineral Petrol* 130:275–287.

Ekelund A. and Engström E. 1990. Detection of cm sized Fe-Mn bodies in rhyolite from Lake Mien, an impact site i Southern Sweden. 19th Lunar and Planetary Science conference. pp. 297–298.

El Goresy A. 1965. Baddeleyite and its significance in impact glasses. *Journal of Geophysical Research* 70:3453–3456.

Engelhardt W. v. and Bertsch W. 1969. Shock induced planar deformation structures in quartz from the Ries crater, Germany. *Contributions to Mineralogy and Petrology* 20:203–234.

Erickson T. M., Cavosie A. J., Moser D. E., Barker I. R., and Radovan H. A. 2013. Correlating planar microstructures in shocked zircon from the Vredefort Dome at multiple scales: Crystallographic modeling, external and internal imaging, and EBSD structural analysis. *American Mineralogist* 98:53–65.

Erickson T. M., Pearce M. A., Reddy S. M., Timms N. E., Cavosie A. J., Bourdet J., Rickard W. D. A., and Nemchin A. A. 2017. Microstructural constraints on the mechanisms of the transformation to reidite in naturally shocked zircon. *Contributions to Mineralogy and Petrology* 172:6.

Erickson T. M., Kirkland C. L., Timms N. E., Cavosie A. J., and Davison T. M. 2020. Precise radiometric age establishes Yarrabubba, Western Australia, as Earth's oldest recognised meteorite impact structure. *Nature Communications* 11:300.

Farley K., Williford K., Stack K., Chen A., Torre M., Hand K., Goreva Y., Herd C., Hueso R., Liu Y., Maki J., Martinez G. M., Moeller R., Nelessen A., Newman C., Nunes D., Ponce A., Spanovich N., and Wiens R. 2020. Mars 2020 Mission Overview. *Space Science Reviews* 216:142.

Farley K. A.Stack K. M.Shuster D. L.Horgan B. H. N.Hurowitz J. A.Tarnas J. D.Simon J. I.Sun V. Z.Scheller E. L.Moore K. R.McLennan S. M.Vasconcelos P. M.Wiens R. C.Treiman A. H.Mayhew L. E.Beyssac

O.Kizovski T. V.Tosca N. J.Williford K. H.Crumpler L. S.Beegle L. W.Bell J. F.Ehlmann B. L.Liu Y.Maki J. N.Schmidt M. E.Allwood A. C.Amundsen H. E. F.Bhartia R.Bosak T.Brown A. J.Clark B. C.Cousin A.Forni O.Gabriel T. S. J.Goreva Y.Gupta S.Hamran S. E.Herd C. D. K.Hickman-Lewis K.Johnson J. R.Kah L. C.Kelemen P. B.Kinch K. B.Mandon L.Mangold N.Quantin-Nataf C.Rice M. S.Russell P. S.Sharma S.Siljeström S.Steele A.Sullivan R.Wadhwa M.Weiss B. P.Williams A. J.Wogsland B. V.Willis P. A.Acosta-Maeda T. A.Beck P.Benzerara K.Bernard S.Burton A. S.Cardarelli E. L.Chide B.Clavé E.Cloutis E. A.Cohen B. A.Czaja A. D.Debaille V.Dehouck E.Fairén A. G.Flannery D. T.Fleron S. Z.Fouchet T.Frydenvang J.Garczynski B. J.Gibbons E. F.Hausrath E. M.Hayes A. G.Henneke J.Jørgensen J. L.Kelly E. M.Lasue J.Le Mouélic S.Madariaga J. M.Maurice S.Merusi M.Meslin P. Y.Milkovich S. M.Million C. C.Moeller R. C.Núñez J. I.Ollila A. M.Paar G.Paige D. A.Pedersen D. A. K.Pilleri P.Pilorget C.Pinet P. C., et al. 2022. Aqueously altered igneous rocks sampled on the floor of Jezero crater, Mars. *Science* 377:eabo2196.

Farmer J. 2000. Hydrothermal systems: Doorways to early biosphere evolution. *GSA Today* 10:1–9.

Fedrigo A., Marstal K., Bender Koch C., Andersen Dahl V., Bjorholm Dahl A., Lyksborg M., Gundlach C., Ott F., and Strobl M. 2018. Investigation of a Monturaqui Impactite by Means of Bi-Modal X-ray and Neutron Tomography. *Journal of Imaging* 4:72.

Ferrière L., Koeberl C., Libowitzky E., Reimold W. U., Greshake A., and Brandstätter F. 2010. Ballen quartz and cristobalite in impactites: New investigations. In *Large Meteorite Impacts and Planetary Evolution IV*, edited by R. L. Gibson and W. U. Reimold, Geological Society of America. pp. 609–618.

Ferrière L., Lubala F. R. T., Osinski G. R., and Kaseti P. K. 2011a. The newly confirmed Luizi impact structure, Democratic Republic of Congo—Insights into central uplift formation and post-impact erosion. *Geology* 39:851–854.

Ferrière L., Lubala R. T., Osinski G., and Kaseti P. 2011b. The Luizi Structure (Democratic Republic of Congo) --- First Confirmed Meteorite Impact Crater in Central Africa.

Fiske P. S. 1999. Shock-induced phase transitions of ZrSiO4, reversion kinetics, and implications for impact heating in terrestrial craters. APS Shock Compression of Condensed Matter Meeting Abstracts. pp. 501.

Floyd C. E., Floyd C. E., Howell C. R., Kapadia A. J., Harrawood B. P., Xia J. Q., and Tourassi G. D. 2004. Neutron-Based Imaging May Lead to Earlier Breast Cancer Diagnosis. 46th Annual Meeting of the American Association of Physicists in Medicine. pp.

French B. M. 1998. *Traces of Catastrophe: A Handbook of shock-Metamorphic Effects in Terrestrial Meteorite Impact Structures*. Lunar and Planetary Institute, Houston. 120 p.

French B. M. and Koeberl C. 2010. The convincing identification of terrestrial meteorite impact structures: What works, what doesn't, and why. *Earth-Science Reviews* 98:123–170.

Friedrich J. M. and Rivers M. L. 2013. Three-dimensional imaging of ordinary chondrite microporosity at 2.6μm resolution. *Geochimica et Cosmochimica Acta* 116:63–70.

Giuli G., Paris E., Pratesi G., Koeberl C., and Cipriani C. 2003. Iron oxidation state in the Fe-rich layer and silica matrix of Libyan Desert Glass: A high-resolution XANES study. *Meteoritics & Planetary Science* 38:1181–1186.

Glass B., Liu S., and Leavens P. 2002. Reidite: An impact-produced high-pressure poly-

morph of zircon found in marine sediments. *American Mineralogist* 87:562–565.

Glass B. P. and Liu S. 2001. Discovery of high-pressure ZrSiO4 polymorph in naturally occurring shock-metamorphosed zircons. *Geology* 29:371–373.

Goderis S. 2011. Projectile identification in terrestrial impact structures and ejecta material

Goderis S., Paquay F., and Claeys P. 2012a. Projectile Identification in Terrestrial Impact Structures and Ejecta Material. In *Impact Cratering: Processes and Products*

edited by G. R. Osinski and E. Pierazzo, Blackwell Publishing Ltd. pp. 223–239.

Goderis S., Paquay F., and Claeys P. 2012b. Projectile Identification in Terrestrial Impact Structures and Ejecta Material. In *Impact Cratering: Processes and Products*, edited by G. R. Osinski and E. Pierazzo, Blackwell Publishing Ltd. pp. 223–239.

Goderis S., Tagle R., Belza J., Smit J., Montanari A., Vanhaecke F., Erzinger J., and Claeys P. 2013. Reevaluation of siderophile element abundances and ratios across the Cretaceous–Paleogene (K–Pg) boundary: Implications for the nature of the projectile. *Geochimica et Cosmochimica Acta* 120:417–446.

Goderis S., Sato H., Ferrière L., Schmitz B., Burney D., Kaskes P., Vellekoop J., Wittmann A., Schulz T., Chernonozhkin S. M., Claeys P., de Graaff S. J., Déhais T., de Winter N. J., Elfman M., Feignon J.-G., Ishikawa A., Koeberl C., Kristiansson P., Neal C. R., Owens J. D., Schmieder M., Sinnesael M., Vanhaecke F., Van Malderen S. J. M., Bralower T. J., Gulick S. P. S., Kring D. A., Lowery C. M., Morgan J. V., Smit J., and Whalen M. T. 2021. Globally distributed iridium layer preserved within the Chicxulub impact structure. *Science Advances* 7:eabe3647.

Gooding J. L., Wentworth S. J., and Zolensky M. E. 1991. Aqueous alteration of the Nakhla meteorite. *Meteoritics* 26:135–143.

Grieve R. and Therriault A. 2012. Impact Cratering: Processes and Products edited by. pp. 90–105.

Grieve R. A. 1997. Extraterrestrial impact events: the record in the rocks and the stratigraphic column. *Palaeogeography, Palaeoclimatology, Palaeoecology* 132:5–23.

Grieve R. A. F., Langenhorst F., and Stöffler D. 1996. Shock metamorphism of quartz in nature and experiment: II. Significance in geoscience*. *Meteoritics & Planetary Science* 31:6–35.

Griffin S., Daly L., Keller T., Piazolo S., Forman L. V., Lee M. R., Baumgartner R. J., Trimby P. W., Benedix G. K., Irving A. J., and Hoefnagels B. 2022. Constraints on the Emplacement of Martian Nakhlite Igneous Rocks and Their Source Volcano From Advanced Micro-Petrofabric Analysis. *Journal of Geophysical Research: Planets* 127:e2021JE007080.

Gucsik A. 2007. Micro-Raman spectroscopy of reidite as an impact-induced high pressure polymorph of zircon: experimental investigation and attempt to application. 47.

Gulick S., Christeson G., McCall N., Morgan J., and Ormö J. 2020. Impactite stratigraphy and depositional processes in the Chicxulub and Ries impact structures: What is a crater floor?

Hallis L. J. and Taylor G. 2011. Comparisons of the four Miller Range nakhlites, MIL 03346, 090030, 090032 and 090136: Textural and compositional observations of primary and secondary mineral assemblages. *Meteoritics & Planetary Science* 46:1787–1803.

Hallis L. J., Taylor G. J., Nagashima K., Huss G. R., Needham A. W., Grady M. M., and Franchi I. A. 2012. Hydrogen isotope analyses of alteration phases in the nakhlite martian meteorites. *Geochimica et Cosmochimica Acta* 97:105–119.

Hamann C., Artemieva N., Wirth R., Roddatis V., and Kearsley A. 2022. Condensation of iron-nickel silicides and silicon monoxide from impact vapor plumes: a case study on the Wabar impact glasses. 85th Annual Meeting of The Meteoritical Society.

Hanna R. D. and Ketcham R. A. 2017. X-ray computed tomography of planetary materials: A primer and review of recent studies. *Geochemistry* 77:547–572.

Henkel H. 1992. Geophysical aspects of meteorite impact craters in eroded shield environment, with special emphasis on electric resistivity. *Tectonophysics* 216:63–89.

Hess K.-U., Flaws A., J. Mühlbauer M., Schillinger B., Franz A., Schulz M., Calzada E., Dingwell D., and Bente K. 2011. *Advances in High-Resolution Neutron Computed Tomography: Adapted to the Earth Sciences*, Geosphere. 1294–1302 p.

Hessenbruch A. 2002. A brief history of x-rays. *Endeavour* 26:137–141.

Hezel D. C., Elangovan P., Viehmann S., Howard L., Abel R. L., and Armstrong R. 2013. Visualisation and quantification of CV chondrite petrography using micro-tomography. *Geochimica et Cosmochimica Acta* 116:33–40.

Hildebrand A. R., Penfield G. T., Kring D. A., Pilkington M., Camargo Z A., Jacobsen S. B., and Boynton W. V. 1991. Chicxulub Crater: A possible Cretaceous/Tertiary boundary impact crater on the Yucatán Peninsula, Mexico. *Geology* 19:867–871.

Holm S., Alwmark C., Alvarez W., and Schmitz B. 2011. Shock barometry of the Siljan impact structure, Sweden. *Meteoritics & Planetary Science* 46:1888–1909.

Holst N. O. 1890. *Ryoliten vid sjön Mien [In Swedish]*. Stockholm, Sveriges Geologiska Undersökning, Serie C. 50 p.

Högbom A. G. 1910. *Geologiska Föreningens Stockholm Förhandlingar* 32.

Kaestner A. P., Hartmann S., Kühne G., Frei G., Grünzweig C., Josic L., Schmid F., and Lehmann E. H. 2011. The ICON beamline – A facility for cold neutron imaging at SINQ. *Nuclear Instruments and Methods in Physics Research Section A: Accelerators, Spectrometers, Detectors and Associated Equipment* 659:387–393.

Kaiser A., Lobert M., and Telle R. 2008. Thermal stability of zircon (ZrSiO4). *Journal of the European Ceramic Society* 28:2199–2211.

Kamo S. L., Lana C., and Morgan J. V. 2011. U–Pb ages of shocked zircon grains link distal K–Pg boundary sites in Spain and Italy with the Chicxulub impact. *Earth and Planetary Science Letters* 310:401–408.

Kardjilov N., Fiori F., Giunta G., Hilger A., Rustichelli F., Strobl M., Banhart J., and Triolo R. 2006. Neutron tomography for archaeological investigations. *Journal of Neutron Research* 14:29–36.

Kardjilov N., Manke I., Woracek R., Hilger A., and Banhart J. 2018. Advances in neutron imaging. *Materials Today* 21:652–672.

Kenkmann T., Collins G. S., and Wünnemann K. 2012. The Modification Stage of Crater Formation. In *Impact Cratering*, edited by. pp. 60–75.

Kenny G. G., Morales L. F., Whitehouse M. J., Petrus J. A., and Kamber B. S. 2017. The formation of large neoblasts in shocked zircon and their utility in dating impacts. *Geology* 45:1003–1006.

Kenny G. G., Mänttäri I., Schmieder M., Whitehouse M. J., Nemchin A. A., Bellucci J. J., and Merle R. E. 2020. Age of the Sääksjärvi impact structure, Finland: reconciling the timing of small impacts in crystalline basement with regional basin development. *Journal of the Geological Society*.

Kiessling W. and Alvarez W. 2002. Distribution of Chicxulub ejecta at the Cretaceous-Tertiary boundary. *Catastrophic events and mass extinctions: Impact and beyond, Spec. Pap. Geol. Soc. Amer* 356:55–68.

Knittle E. and Williams Q. 1993. High-pressure Raman spectroscopy of ZrSiOoz Observation of the zircon to scheelite transition at 300 K. *American Mineralogist* 78:245–252.

Koeberl C. 1998. Identification of meteoritic components in impactites. *Geological Society, London, Special Publications* 140:133–153.

Koeberl C. 1999. Craters On The Moon From Galileo To Wegener: A Short History Of The Impact Hypothesis, And Implications For The Study Of Terrestrial Impact Craters. *Earth, Moon, and Planets* 85:209–224.

Koeberl C. 2000. Confirmation of a Meteoritic Component in Libyan Desert Glass from Osmium-Isotopic Data. *Meteoritics & Planetary Science* 35:A89–A90.

Koeberl C., Denison C., Ketcham R., and Reimold W. 2002. High-resolution X-ray computed tomography of impactites. *Journal of Geophysical Research* 107.

Koeberl C., Schulz T., and Reimold W. U. 2015. Remnants of Early Archean Impact Deposits on Earth: Search for a Meteoritic Component in the BARB5 and CT3 Drill Cores (Barberton Greenstone Belt, South Africa). *Procedia Engineering* 103:310–317.

Koeberl C. and Ferrière L. 2019. *Libyan Desert Glass area in western Egypt: Shocked quartz in bedrock points to a possible deeply eroded impact structure in the region* p.

Kring D. 2003. Environmental Consequences of Impact Cratering Events as a Function of Ambient Conditions on Earth. *Astrobiology* 3:133–152.

Kring D. A. 2000. Impact-induced hydrothermal activity and potential habitats for thermophilic and hyperthermophilic life. Catastrophic Events and Mass Extinctions: Impacts and Beyond,. pp. 106–107.

Kring D. A. and Cohen B. A. 2002. Cataclysmic bombardment throughout the inner solar system 3.9–4.0 Ga. *Journal of Geophysical Research: Planets* 107:4–1–4–6.

Krzesińska A. 2011. High resoIution X-ray tomography as a tool for analysis of internal textures in meteorites. *Meteorites* 01:3–12.

Kusaba K., Syono Y., Kikuchi M., and Fukuoka K. 1985. Shock behavior of zircon; phase transition to scheelite structure and decomposition. *Earth and Planetary Science Letters* 72:433–439.

Le Feuvre M. and Wieczorek M. A. 2011. Nonuniform cratering of the Moon and a revised crater chronology of the inner Solar System. *Icarus* 214:1–20.

Lee S. R., Horton Jr J. W., and Walker R. J. 2006. Confirmation of a meteoritic component in impact-melt rocks of the Chesapeake Bay impact structure, Virginia, USA—Evidence from osmium isotopic and PGE systematics. *Meteoritics & Planetary Science* 41:819–833.

Leroux H., Reimold W. U., Koeberl C., Hornemann U., and Doukhan J. C. 1999. Experimental shock deformation in zircon: a transmission electron microscopic study. *Earth and Planetary Science Letters* 169:291–301.

Mannes D., Schmid F., Frey J., Schmidt-Ott K., and Lehmann E. 2015. Combined Neutron and X-ray Imaging for Non-invasive Investigations of Cultural Heritage Objects. *Physics Procedia* 69:653–660.

Markwitz V., Kirkland C. L., Mehnert A., Gessner K., and Shaw J. 2017. 3-D Characterization of Detrital Zircon Grains and its Implications for Fluvial Transport, Mixing, and Preservation Bias. *Geochemistry, Geophysics, Geosystems* 18:4655–4673.

Martell J., Alwmark C., Alwmark S., Hall S., Hektor J., Woracek R., Helfen L., and Tengattini A. 2021a. Neutron tomography as a tool for pin-pointing meteoritic

components in impactites. 52nd Lunar and Planetary Science Conference.

Martell J., Alwmark C., Holm-Alwmark S., and Lindgren P. 2021b. Shock deformation in zircon grains from the Mien impact structure, Sweden. *Meteoritics & Planetary Science* 56:362–378.

Matsumoto T., Tsuchiyama A., Nakamura-Messenger K., Nakano T., Uesugi K., Takeuchi A., and Zolensky M. E. 2013. Three-dimensional observation and morphological analysis of organic nanoglobules in a carbonaceous chondrite using X-ray micro-tomography. *Geochimica et Cosmochimica Acta* 116:84–95.

McIntyre D. B. 1962. Impact metamorphism at Clearwater Lake, Quebec. *Journal of Geophysical Research* 67:1647–1647.

Melosh H. J. 1989. *Impact cratering : a geologic process*. New York : Oxford University Press, 1989 p.

Morgan J. V., Gulick S. P., Bralower T., Chenot E., Christeson G., Claeys P., Cockell C., Collins G. S., Coolen M. J., and Ferrière L. 2016. The formation of peak rings in large impact craters. *Science* 354:878–882.

Moser D. E., Cupelli C. L., Barker I. R., Flowers R. M., Bowman J. R., Wooden J., and Hart J. R. 2011. New zircon shock phenomena and their use for dating and reconstruction of large impact structures revealed by electron nanobeam (EBSD, CL, EDS) and isotopic U–Pb and (U–Th)/He analysis of the Vredefort dome. *Canadian Journal of Earth Sciences* 48:117–139.

Mustard J. F., Murchie S. L., Pelkey S. M., Ehlmann B. L., Milliken R. E., Grant J. A., Bibring J. P., Poulet F., Bishop J., Dobrea E. N., Roach L., Seelos F., Arvidson R. E., Wiseman S., Green R., Hash C., Humm D., Malaret E., McGovern J. A., Seelos K., Clancy T., Clark R., Marais D. D., Izenberg N., Knudson A., Langevin Y., Martin T., McGuire P., Morris R., Robinson M., Roush T., Smith M., Swayze G., Taylor H., Titus T., and Wolff M. 2008. Hydrated silicate minerals on Mars observed by the Mars Reconnaissance Orbiter CRISM instrument. *Nature* 454:305–309.

Needham A., Abel R., Tomkinson T., and Grady M. 2013. Martian subsurface fluid pathways and 3D mineralogy of the Nakhla meteorite. *Geochimica et Cosmochimica Acta* 116:96–110.

Needham A. W., Bilheux H. Z., Eckley S. A., and Zeigler R. A. 2020. Coordinated Analyses of Chondrites Using Neutron and X-Ray Computed Tomography, and Electron Microscopy. 51st Lunar and Planetary Science Conference.

Nilsson B. 2003. *Tingens och tankarnas landskap: försök i naturumgängets arkeologi med exempel ur Blekinges och Smålands förflutna*. Lund University p.

Nyquist L. E., Bogard D. D., Shih C. Y., Greshake A., Stöffler D., and Eugster O. 2001. Ages and Geologic Histories of Martian Meteorites. *Space Science Reviews* 96:105–164.

Osinski G. R., Tornabene L. L., Banerjee N. R., Cockell C. S., Flemming R., Izawa M. R. M., McCutcheon J., Parnell J., Preston L. J., Pickersgill A. E., Pontefract A., Sapers H. M., and Southam G. 2013. Impact-generated hydrothermal systems on Earth and Mars. *Icarus* 224:347–363.

Osinski G. R. and Grieve R. A. F. 2017. "Suevites" of the West Clearwater Lake Impact Structure, Canada: A demonstration of the need for a revised classification scheme for impactites (abstract #2381). 48th Lunar and Planetary Science Conference.

Osinski G. R., Cockell C. S., Pontefract A., and Sapers H. M. 2020. The Role of Meteorite Impacts in the Origin of Life. *Astrobiology* 20:1121–1149.

Osinski G. R., Grieve R. A. F., Ferrière L., Losiak A., Pickersgill A., Cavosie A. J., Hibbard S. M., Hill P., Bermudez J. J., Marion

C. L., Newman J. D., and Simpson S. L. 2022. Impact Earth: A review of the terrestrial impact record. *Earth-Science Reviews*104112.

Pakhnevich A. 2016. On the application of tomography techniques to search for water and organic matter in meteorites. Bruker microCT User Meeting.

Pakhnevich A., Kurkin A., Lavrov A., Tarasenko K., Kovalenko E., Kaloyan A., and Podurets K. 2018. Synchrotron and Neutron Tomography of Paleontological Objects on the Facilities of the Kurchatov Institute. *Journal of Imaging* 4:103.

Palme H., Janssens M.-J., Takahashi H., Anders E., and Hertogen J. 1978. Meteoritic material at five large impact craters. *Geochimica et Cosmochimica Acta* 42:313–323.

Peetermans S., Grazzi F., Salvemini F., Lehmann E. H., Caporali S., and Pratesi G. 2013. Energy-selective neutron imaging for morphological and phase analysis of iron–nickel meteorites. *Analyst* 138:5303–5308.

Plan A., Kenny G. G., Erickson T. M., Lindgren P., Alwmark C., Holm-Alwmark S., Lambert P., Scherstén A., and Söderlund U. 2021. Exceptional preservation of reidite in the Rochechouart impact structure, France: New insights into shock deformation and phase transition of zircon. *Meteoritics & Planetary Science* 56:1795–1828.

Potter R. W. K. 2015. Investigating the onset of multi-ring impact basin formation. *Icarus* 261:91–99.

Pratesi G., Viti C., Cipriani C., and Mellini M. 2002. Silicate-silicate liquid immiscibility and graphite ribbons in Libyan desert glass. *Geochimica et Cosmochimica Acta* 66:903–911.

Prior D. J., Mariani E., and Wheeler J. 2009. EBSD in the earth sciences: applications, common practice, and challenges. In *Electron backscatter diffraction in materials science*, edited by, Springer. pp. 345–360.

Quitté G., Robin E., Levasseur S., Capmas F., Rocchia R., Birck J. L., and Allègre C. J. 2007. Osmium, tungsten, and chromium isotopes in sediments and in Ni□rich spinel at the K□T boundary: Signature of a chondritic impactor. *Meteoritics & Planetary Science* 42:1567–1580.

Ramkissoon N. K., Turner S. M. R., Macey M. C., Schwenzer S. P., Reed M. H., Pearson V. K., and Olsson-Francis K. 2021. Exploring the environments of Martian impact-generated hydrothermal systems and their potential to support life. *Meteoritics & Planetary Science* n/a.

Reddy S. M., Johnson T. E., Fischer S., Rickard W. D. A., and Taylor R. J. M. 2015. Precambrian reidite discovered in shocked zircon from the Stac Fada impactite, Scotland. *Geology* 43:899–902.

Rogers J. D. 2013. The Neutron's Discovery - 80 Years on. *Physics Procedia* 43:1–9.

Schindelin J., Arganda-Carreras I., Frise E., Kaynig V., Longair M., Pietzsch T., Preibisch S., Rueden C., Saalfeld S., Schmid B., Tinevez J.-Y., White D. J., Hartenstein V., Eliceiri K., Tomancak P., and Cardona A. 2012. Fiji: an open-source platform for biological-image analysis. *Nature Methods* 9:676–682.

Schmieder M. and Jourdan F. 2013. The Lappajärvi impact structure (Finland): Age, duration of crater cooling, and implications for early life. Geochimica et Cosmochimica Acta 112:321-339. https://doi.org/10.1016/j.gca.2013.02.015.

Schmieder M., Tohver E., Jourdan F., Denyszyn S. W., and Haines P. W. 2015. Zircons from the Acraman impact melt rock (South Australia): Shock metamorphism, U–Pb and 40Ar/39Ar systematics, and implications for the isotopic dating of impact events. *Geochimica et Cosmochimica Acta* 161:71–100.

Schmieder M. and Kring D. 2020. Earth's Impact

Events Through Geologic Time: A List of Recommended Ages for Terrestrial Impact Structures and Deposits. *Astrobiology* 20:91–141.

Schulte P., Alegret L., Arenillas I., Arz J. A., Barton P. J., Bown P. R., Bralower T. J., Christeson G. L., Claeys P., Cockell C. S., Collins G. S., Deutsch A., Goldin T. J., Goto K., Grajales-Nishimura J. M., Grieve R. A. F., Gulick S. P. S., Johnson K. R., Kiessling W., Koeberl C., Kring D. A., MacLeod K. G., Matsui T., Melosh J., Montanari A., Morgan J. V., Neal C. R., Nichols D. J., Norris R. D., Pierazzo E., Ravizza G., Rebolledo-Vieyra M., Reimold W. U., Robin E., Salge T., Speijer R. P., Sweet A. R., Urrutia-Fucugauchi J., Vajda V., Whalen M. T., and Willumsen P. S. 2010. The Chicxulub Asteroid Impact and Mass Extinction at the Cretaceous-Paleogene Boundary. *Science* 327:1214–1218.

Sears D. W. G., Sears H., Ebel D. S., Wallace S., and Friedrich J. M. 2016. X-ray computed tomography imaging: A not-so-nondestructive technique. *Meteoritics & Planetary Science* 51:833–838.

Sharp T. G. and DeCarli P. S. 2006. *Shock Effects in Meteorites*. Tuscon, University of Arizona press p.

Sighinolfi G. P., Lugli F., Piccione F., Michele V. D. E., and Cipriani A. 2020. Terrestrial target and melting site of Libyan Desert Glass: New evidence from trace elements and Sr isotopes. *Meteoritics & Planetary Science* n/a.

Smit J. and Hertogen J. 1980. An extraterrestrial event at the Cretaceous–Tertiary boundary. *Nature* 285:198–200.

Stamati O., Andò E., Roubin E., Cailletaud R., Wiebicke M., Pinzon G., Couture C., Hurley R., Caulk R., Caillerie D., Matsushima T., Bésuelle P., Bertoni F., Arnaud T., Laborin A., Rorato R., Yue S., Tengattini A., Okubadejo O., and Birmpilis G. 2020. spam: Software for Practical Analysis of Materials. *Journal of Open Source Software* 5:2286.

Steen Duchnik S., Lanzky M., and Steffensen Schmidt L. 2012. X-ray and Neutron Tomography of the Allende Meteorite. Bachelor Thesis, Niels Bohr Institute, Copenhagen University.

Stöffler D. 1966. Zones of impact metamorphism in the crystalline rocks of the Nördlinger Ries crater. *Contributions to Mineralogy and Petrology* 12:15–24.

Stöffler D. and Langenhorst F. 1994. Shock metamorphism of quartz in nature and experiment: I. Basic observation and theory*. *Meteoritics* 29:155–181.

Stöffler D., Hamann C., and Metzler K. 2018. Shock metamorphism of planetary silicate rocks and sediments: Proposal for an updated classification system. *Meteoritics & Planetary Science* 53:5–49.

Suuronen J. P. and Sayab M. 2018. 3D nanopetrography and chemical imaging of datable zircons by synchrotron multimodal X-ray tomography. *Scientific Reports* 8:4747.

Svensson N. B. and Wickman F. E. 1965. Coesite from Lake Mien, Southern Sweden. *Nature* 205:1202–1203.

Söderlund U. and Johansson L. 2002. A simple way to extract baddeleyite (ZrO2). *Geochemistry, Geophysics, Geosystems* 3:1–7.

Tagle R., Erzinger J., Hecht L., Schmitt R. T., Stöffler D., and Claeys P. 2004. Platinum group elements in impactites of the ICDP Chicxulub drill core Yaxcopoil-1: Are there traces of the projectile? *Meteoritics & Planetary Science* 39:1009–1016.

Tait K. T., McCubbin F. M., C. L. Smith, C.B. Agee, H. Busemann, B. Cavalazzi, Vinciane. Debaille, Aurore Hutzler, Tomohiro Usui, Gerhard Kminek, Michael A. Meyer, David W. Beaty, Brandi L. Carrier, Timothy Haltigin, Lindsay E. Hays, Charles S. Cockell, Daniel P. Glavin,

Monica M. Grady, Ernst Hauber, Bernard Marty, Lisa M. Pratt, Aaron B. Regberg, Alvin L. Smith, Roger E. Summons, Timothy D. Swindle, Nicholas J. Tosca, Arya Udry, Michael A. Velbel, Meenakshi Wadhwa, Frances Westall, and Zorzano. M.-P. 2022. Preliminary Planning for Mars Sample Return (MSR) Curation Activities in a Sample Receiving Facility (SRF). *Astrobiology* 22:S–57–S–80.

Tengattini A., Lenoir N., Andò E., Giroud B., Atkins D., Beaucour J., and Viggiani G. 2020a. NeXT-Grenoble, the Neutron and X-ray tomograph in Grenoble. *Nuclear Instruments and Methods in Physics Research Section A: Accelerators, Spectrometers, Detectors and Associated Equipment* 968:163939.

Tengattini A., Lenoir N., Andò E., and Viggiani G. 2020b. Neutron imaging for geomechanics: A review. *Geomechanics for Energy and the Environment*100206.

Timms N. E., Reddy S. M., Healy D., Nemchin A. A., Grange M. L., Pidgeon R. T., and Hart R. 2012. Resolution of impact-related microstructures in lunar zircon: A shock-deformation mechanism map. *Meteoritics & Planetary Science* 47:120–141.

Treiman A., LaManna J., Hussey D., deClue I., and Anovitz L. 2022. Coordinated neutron and X-ray computed tomography of meteorites: Detection and distribution of hydrogen-bearing materials. *Meteoritics & Planetary Science* 57:1820–1835.

Treiman A. H., Barrett R. A., and Gooding J. L. 1993. Preterrestrial aqueous alteration of the Lafayette (SNC) meteorite. *Meteoritics* 28:86–97.

Treiman A. H. 2005. The nakhlite meteorites: Augite-rich igneous rocks from Mars. *Geochemistry* 65:203–270.

Treiman A. H., LaManna J. M., Anovitz L. M., Hussey D. S., and Jacobson D. L. 2018. Neutron Computed Tomography of Meteorites: Detecting Hydrogen-Bearing Materials. 49th Lunar and Planetary Science Conference.

Tsuchiyama A., Nakamura T., Nakano T., and Nakamura N. 2002. Three-dimensional description of the Kobe meteorite by micro X-ray CT method: Possibility of three-dimensional curation of meteorite samples. *GEOCHEMICAL JOURNAL* 36:369–390.

Udry A. and Day J. M. D. 2018. 1.34 billion-year-old magmatism on Mars evaluated from the co-genetic nakhlite and chassignite meteorites. *Geochimica et Cosmochimica Acta* 238:292–315.

von Engelhardt W. and Stöffler D. 1965. Spaltflächen im Quarz als Anzeichen für Einschläge großer Meteoriten. *Naturwissenschaften* 52:489–490.

Watson L. L., Hutcheon I. D., Epstein S., and Stolper E. M. 1994. Water on Mars: Clues from Deuterium/Hydrogen and Water Contents of Hydrous Phases in SNC Meteorites. *Science* 265:86.

Welzenbach L. C., Fries M. D., Grady M. M., Greenwood R. C., McCubbin F. M., Zeigler R. A., Smith C. L., and Steele A. 2017. X-Ray Computed Tomography: The First Step in Mars Sample Return Processing. 48th Lunar and Planetary Science Conference. pp.

Wiechert U., Halliday A. N., Lee D. C., Snyder G. A., Taylor L. A., and Rumble D. 2001. Oxygen Isotopes and the Moon-Forming Giant Impact. *Science* 294:345–348.

Wilde S. A., Valley J. W., Peck W. H., and Graham C. M. 2001. Evidence from detrital zircons for the existence of continental crust and oceans on the Earth 4.4 Gyr ago. *Nature* 409:175–178.

Wilkins J. 1638. *The Discovery of a World in the Moone: Or A Discourse Tending To Prove that 'tis probable there may be another habitable World in that Planet.* London: Printed by E. G. for Michael Sparke and Edward Forrest p.

Wittmann A., Kenkmann T., Schmidt R. T., and Stöffler D. 2006. Shock-metamorphosed zircon in terrestrial impact craters. *Meteoritics & Planetary Science* 41:433–454.

Yada T.Abe M.Okada T.Nakato A.Yogata K.Miyazaki A.Hatakeda K.Kumagai K.Nishimura M.Hitomi Y.Soejima H.Yoshitake M.Iwamae A.Furuya S.Uesugi M.Karouji Y.Usui T.Hayashi T.Yamamoto D.Fukai R.Sugita S.Cho Y.Yumoto K.Yabe Y.Bibring J.-P.Pilorget C.Hamm V.Brunetto R.Riu L.Lourit L.Loizeau D. Lequertier G.Moussi-Soffys A.Tachibana S.Sawada H.Okazaki R.Takano Y.Sakamoto K.Miura Y. N.Yano H.Ireland T. R.Yamada T.Fujimoto M.Kitazato K.Namiki N.Arakawa M.Hirata N.Yurimoto H.Nakamura T.Noguchi T.Yabuta H.Naraoka H.Ito M.Nakamura E.Uesugi K.Kobayashi K.Michikami T.Kikuchi H.Hirata N.Ishihara Y.Matsumoto K.Noda H.Noguchi R.Shimaki Y.Shirai K.Ogawa K.Wada K.Senshu H.Yamamoto Y.Morota T.Honda R.Honda C.Yokota Y.Matsuoka M.Sakatani N.Tatsumi E.Miura A.Yamada M.Fujii A.Hirose C.Hosoda S.Ikeda H.Iwata T.Kikuchi S.Mimasu Y.Mori O.Ogawa N.Ono G.Shimada T.Soldini S. Takahashi T.Takei Y.Takeuchi H.Tsukizaki R.Yoshikawa K.Terui F.Nakazawa S.Tanaka S.Saiki T.Yoshikawa M., et al. 2022. Preliminary analysis of the Hayabusa2 samples returned from C-type asteroid Ryugu. *Nature Astronomy* 6:214–220.

Zeigler R. A., Almeida N., Sykes D., and Smith C. 2014. X-ray microcomputed tomography of Apollo samples as a curation technique enabling better research. 77th Annual Meteoritical Society Meeting.

Zhang J., Dauphas N., Davis A. M., Leya I., and Fedkin A. 2012. The proto-Earth as a significant source of lunar material. *Nature Geoscience* 5:251–255.

Zubov A. A., Shumilova T. G., Zhuravlev A. V., and Isaenko S. I. 2021. X-ray computed microtomography of diamondiferous impact suevitic breccia and clast-poor melt rock from the Kara astrobleme (Pay-Khoy, Russia). *American Mineralogist* 106:1860–1870.

Åström K. 1998. Seismic signature of the Lake Mien impact structure, southern Sweden. *Geophysical Journal International* 135:215–231.

Litholund Theses

Dissertations

1. *Emma F. Rehnström,* 2003: Geography and geometry of pre-Caledonian western Baltica: U-Pb geochronology and palaeomagnetism.

2. *Oskar Paulsson,* 2003: U-Pb geochronology of tectonothermal events related to the Rodinia and Gondwana supercontinents: observations from Antarctica and Baltica.

3. *Ingela Olsson-Borell,* 2003: Thermal history of the Phanerozoic sedimentary succession of Skåne, southern Sweden, and implications for applied geology.

4. *Johan Lindgren,* 2004: Early Campanian mosasaurs (Reptilia; Mosasauridae) from the Kristianstad Basin, southern Sweden.

5. *Audrius Cecys,* 2004: Tectonic implications of the ca. 1.45 Ga granitoid magmatism at the southwestern margin of the East European Craton.

6. *Peter Dahlqvist,* 2005: Late Ordovician-Early Silurian facies development and stratigraphy of Jämtland, central Sweden.

7. *Mårten Eriksson,* 2005: Silurian carbonate platform and unconformity development, Gotland, Sweden.

8. *Jane Wigforss-Lange,* 2005: The effects of Late Silurian (mid-Ludfordian) sea-level change: a case study of the Öved-Ramsåsa Group in Skåne, Sweden.

9. *Erik Eneroth,* 2006: Nanomagnetic and micromagnetic properties of rocks, minerals and sulphide-oxidation products.

10. *Niklas Axheimer,* 2006: The lower and middle Cambrian of Sweden: trilobites, biostratigraphy and intercontinental correlation.

11. *Fredrik Terfelt,* 2006: Upper middle Cambrian through Furongian of Scandinavia with focus on trilobites, paleoenvironments and correlations.

12. *Andrius Rimsa,* 2007: Understanding zircon geochronology: constraints from imaging and trace elements.

13. *Mårten Eriksson* 2007: Silurian carbonate platforms of Gotland, Sweden: archives of local, regional and global environmental changes.

14. *Jane Wigforss-Lange,* 2007: Geochemical and sedimentary signatures of Phanerozoic events.

15. *Tobias Hermansson,* 2007: The tectonic evolution of the western part of the Svecofennian orogen, central Sweden: Insight from U/Pb and $^{40}Ar/^{39}Ar$ geochronology at Forsmark.

16. *Pia Söderlund,* 2008: ^{40}Ar-^{39}Ar, AFT and (U-Th)/He thermochronologic implications for the low-temperature geological evolution in SE Sweden.

17. *Anders Cronholm,* 2009: The flux of extraterrestrial matter to Earth as recorded in Paleogene and Middle Ordovician marine sediments.

18. *Carl Alwmark,* 2009: Traces in Earth's geological record of the break-up of the L-chondrite parent body 470 Ma.

19. *Linda Larsson-Lindgren,* 2009: Climate and vegetation during the Miocene: evidence from Danish palynological assemblages.

20. *Ingemar Bergelin,* 2010: $^{40}Ar/^{39}Ar$ whole-rock geochronology of Mesozoic basalts in Scania: evidence for episodic volcanism over an extended period of ca. 80 Myr.

21. *Johanna Mellgren,* 2011: Conodont biostratigraphy, taxonomy and palaeoecology in the Darriwilian (Middle Ordovician) of Baltoscandia: with focus on meteorite and extraterrestrial chromite-rich strata.

22. *Johan Olsson,* 2012: U-Pb baddeleyite geochronology of Precambrian mafic dyke swarms and complexes in southern Africa: regional-scale extensional events and the origin of the Bushveld complex.

23. *Kristina Mehlqvist,* 2013: Early land plant spores from the Paleozoic of Sweden : taxonomy, stratigraphy and paleoenvironments.

24. *Andreas Petersson,* 2015: Evolution of continental crust in the Proterozoic: growth and reworking in orogenic systems.

25. *Karolina Bjärnborg,* 2015: Origin of the Kleva Ni-Cu sulphide mineralisation in Småland, southeast Sweden.

26. *Lorraine Tual,* 2016: P–T evolution and high-temperature deformation of Precambrian eclogite, Sveconorwegian orogen.

27. *Mimmi Nilsson,* 2016: New constraints on paleoreconstructions through geochronology of mafic dyke swarms in North Atlantic Craton.

28. *Sanna Alwmark,* 2016: Terrestrial consequences of hypervelocity impact: shock metamorphism, shock barometry, and newly discovered impact structures.

29. *Anders Lindskog,* 2017: Early–Middle Ordovician biotic and sedimentary dynamics in the Baltoscandian paleobasin.

30. *Ashley Gumsley*, 2017: Validating the existence of the supercraton Vaalbara in the Mesoarchaean to Palaeoproterozoic.

31. *Johan Gren,* 2018: Molecular, micro- and ultrastructural investigations of labile tissues in deep time.

32. *Elisabeth Einarsson,* 2018: Palaeoenvironments, palaeoecology and palaeobiogeography of Late Cretaceous (Campanian) faunas from the Kristianstad Basin, southern Sweden, with applications for science education.

33. *Victoria Beckman,* 2018: Metamorphic zircon formation in gabbroic rocks: the tale of microtextures.

34. *Maria Herrmann,* 2020: Geochronology of impact structures - constraining syn- and post-impact processes using the $^{40}Ar/^{39}Ar$ and U-Pb techniques.

35. *Miriam Heingård,* 2022: Exceptional fossil preservation: implications for palaeobiology and taphonomy.

36. *Randolph De La Garza*, 2022: Preservation of Marine Reptile Soft Parts: Reconstructing the Life and Death of Ancient Leviathans.

37. *Josefin Martell*, 2022: Leave no trace: A non-destructive correlative approach providing new insights into impactites and meteorites.

Printed by Media-Tryck, Lund 2022 NORDIC SWAN ECOLABEL 3041 0903

Lake Mien

Lithosphere and Biosphere Science
Department of Geology
Lund University
Sölvegatan 12
SE-223 62 Lund, Sweden
Telephone +46 46 222 78 80

ISSN 1651-6648
ISBN 978-91-87847-68-4